博士論文(要約)

Tracking data reveal seabirds' locomotion strategies in response to wind
(経路データから明らかにする海鳥の風に対する長距離移動戦略)

後藤 佑介

INDEX

CHAPTER1

General introduction

Bird movement response to wind should significantly affect on its travel duration, energy expenditure and probability the birds can reach destination properly, and, hence, these effects will influence the fitness of the individuals (Chapman et al. 2011). Bird movement response to wind is characterized by external factor (wind) and internal factors (Nathan et al. 2008). Internal factors can be categorized to some components. The First component is movement strategy of birds. The birds' adjustment of their heading and airspeed and large-scale path planning in response to wind patterns can significantly affect on the time and energetic cost of the travel (Alerstam and Lindström 1990, McLaren et al. 2014, 2016, Chapman et al. 2016). To enable these movement strategies, the other components of birds' internal factors play important role. The first is navigation capacity; the ability of birds to sense their locations and/or wind direction and speed (Kramer 1953, Chapman et al. 2015). The second is movement capacity of birds; the flight style of birds such as flapping, gliding and thermal soaring and dynamic soaring (Norberg 2012). In the following, details of these components and which areas of these components have been intensively studied (or not studied) are explained.

The movement strategy of birds relates to two effects of wind components; tailwind and crosswind components. Tailwind component increases the ground speed of birds and, hence, reduces time and energy cost to reach the goal (Butler et al. 1997, Liechti and Bruderer 1998, Weber and Hedenström 2000). Many studies reported migrating birds tend to depart their stopover sites when wind is blowing to their destination (Åkesson and Hedenström 2000, Dänhardt and Lindström 2001, Åkesson et al. 2002). Overall, birds prefer tailwind as it assists their travel (Fig. 1-1A). However, perfect tailwind condition (wind direction coincides with the preferred direction) may be rare and there may exist some degree of crosswind component. The crosswind component is, on the contrary, unfavorable for birds as it deviates bird's track from intended course.

To deal with this crosswind effect, the bird should adjust its heading to windward, that is called wind compensation. An illustrative example of a bird response to flow can be constructed in which the bird's preferred direction is northwards but the wind is blowing approximately eastwards. If a bird is to align its heading vector (the bird's speed and direction relative to the surrounding fluid, hereafter referred to as the heading speed and heading, respectively) with the preferred direction (northwards), the direction of the track vector (the bird's speed and direction relative to the ground) would be northeast, deviating from the preferred direction (Fig. 1-1B). In other words, the bird would be drifting due to the flow (known as full drift). The bird would be able to reduce the drift by directing its heading vector point somewhat into the flow (Fig. 1-1CD). This is generally referred to as flow compensation. Especially, in the case in which the bird's track direction coincides with the preferred direction, it is known as complete compensation (Fig. 1-1D) and, otherwise, partial compensation (Fig. 1-1C). The compensation for flow drift is a adaptive response to crosswind as it increases the reliability of the bird reaching its destination and reduces the time spent travelling and thus minimizes its total energy cost (Chapman et al. 2011, McLaren et al. 2016). Our understanding of wind compensation of birds has been developed by studies using radar (Lack 1958) and recent advanced animal tracking techniques. All three movement strategies mentioned above (full drift, partial compensation and full compensation) has been observed. Especially, whether birds can compensate wind above the open sea has been an interested problem since the pioneering work of David Lack as it provides us the knowledge about their navigation capacities (Lack 1958, Alerstam and Ulfstrand 1974, Alerstam 1975, 1976). Birds flying over land are expected to use landmarks for referencing their position relative to the ground to prevent drifting due to lateral wind. Contrary to this, birds moving over the ocean such as seabirds, where landmarks are absent, do not have any referencing beacons (Alerstam 1976). Hence, if birds flying over the sea showed wind compensation, it indicates birds have map sense that they can know their location relative to their goal without visual cues (Kramer 1953, Able 2001, Orchan et al. 2016).

However, the approach investigating birds navigation capacity from response to wind of free-ranging birds flying landmark poor environment have been rare (One of the hindrances was technical difficulty to acquire detailed wind and bird orientation information as radar sites are restricted on land). Rather, the navigation capacity of birds has been intensively studied by experiment using caged birds and anatomical and physiological approaches. Using the caged bird and artificially controlling the external cues, it was shown that birds use directional information from cues the such as sun (Kramer 1952) and stars (Emlen 1967a, 1967b) and even the Earth's magnetic field (Wiltschko et al. 1971, Wiltschko and Wiltschko 1972). Magnetic information is also considered to be important for animals to find their location, i.e. map sense. In loggerhead sea turtles and Caribbean spiny lobsters, use of magnetic cues for map was supported by exposing animals in water-filled arena to altered magnetic field that corresponds to that of the distant locations and investigation their moving direction (Fischer et al. 2001, Lohmann et al. 2001, Boles and Lohmann 2003). In birds homing pigeon was used to test the use of magnetic map. Although use of geomagnetic cues for map sense was partially supported, there are possibility that olfactory cues and landmarks also play important roles (Gagliardo et al. 2009, Wiltschko et al. 2009). Our understanding on physiological and molecular mechanism of birds to sensor magnetic field has been also advanced last few decades. There are two promising candidate mechanisms. First one is using ferromagnetic materials. Anatomical studies revealed clusters of ferromagnetic materials exist in upper beak of pigeons (Fleissner et al. 2003, 2007). Pulse remagnetization that apply a brief, strong magnetic pulse to bird changed their behavior and this result also support the ferromagnetic sensor (Wiltschko et al. 1994, Beason et al. 1995, Holland et al. 2009). The second candidate is magnetically sensitive biochemical reactions that proceed via light-induced electron transfer between two molecules (Ritz et al. 2000, Maeda et al. 2008, 2012). Identified ultraviolet/violet cones in birds' eye as a probable magnetroreceptors (Nießner et al. 2011).

The movement capacity is another important component that underpin the birds movement strategy

in relation to wind. The movement capacities of birds itself have been intensively studied both theoretically and experimentally in the field of biomechanics (Dickinson et al. 2000, Videler et al. 2004, Pennycuick 2008, Norberg 2012). On the other hand, the integrative understanding on how movement capacity of birds affect on their movement strategy in response to wind seems to be poor. For example, in the movement strategies of birds in response to wind, birds' flight style is implicitly assumed to be flapping flight. However, if birds adopt different flight style such as formation flight exploiting upwash generated by other birds (Portugal et al. 2014) or soaring that exploit updraft (Weimerskirch et al. 2016) or wind shear on the sea (Sachs 2004), the optimal movement strategy of birds can change from that of simple flapping flier.

In this study, the movement of seabirds in response to wind is studied. Seabirds have some unique points worth to be studied and potentially enhance our knowledge about the unrevealed area of movement strategy in response to wind, navigation capacity and movement capacity of birds. In chapter 2, whether seabirds could compensate crosswind was investigated. As mentioned above, movement strategy of birds in response to wind over the sea has been important problem yet to be investigated. Here, homing tracks of streaked shearwaters (*Calonectris leucomelas*) was analyzed. In homing, birds were flying in cross wind, and which orientation strategy (Fig. 1-1B,C, and D) in response to cross wind did birds adopt was investigated. In chapter 3, it is shown that movement capacity (flight style) of birds can drastically change the movement strategy of birds. Wandering albatrosses (*Diomedea exulans*) avoided tailwind even if wind was blowing to their goal (Fig. 1-1A) and showed large-scale zigzag movement. Using physical model for soaring birds, it was revealed that their curious movement stems from their unique soaring flight style and tailwind avoidance is an efficient homing way for soaring birds.

In both chapter, wind and birds' heading vector are important information but difficult to directly measure. This technical difficulty is one of the reasons that hindered the advance of our understanding of birds' movement in response. To overcome this difficulty, I employed an "inverse problem approach" to estimate

the causal factors affecting animal movement by using their tracks to quantify navigational decisions in response to environmental disturbance (e.g., wind). The inverse problem approach is widely used in physics and engineering to estimate unobservable causal factors from observed output data (Groetsch 1993). However, the use of this approach remains uncommon in biology (Ishihara and Sugimura 2012, Kondo et al. 2013), especially in animal ecology, because it requires sufficiently large datasets. Another important hindrance is the lack of relevant underlying theory that describes how the model and its parameters that are to be inferred relate to the datasets. The bio-logging technique, whereby data loggers are attached temporarily to free-living animals in the wild, and the high-resolution data it produces now enables the use of the inverse problem approach in this research field. In the first part of chaphter 2, a new method was proposed to estimate both heading and flow vectors to reveal animal decision-making in response to the flow, using tracking data only based on the inverse problem approach. For this, a model is needed that quantitatively relates the observation data (i.e., track data) with the parameters to be estimated (i.e., heading and wind vectors). Such a model was constructed by using a (Biased) Random Walk model, one of the basic theories for animal movement analysis that describe the direction and length of the animal track vector using probability densities (Turchin 1998, Okubo and Levin 2001, Codling et al. 2008, Benhamou 2014). A model introduced in chapter 2 is simple model that added flow effect to Biased Random walk. The method is applied to the homing tracks of streaked shearwaters recorded at a resolution of one location per minute. Although the wind was successfully estimated, the simple model required to assume the wind and heading vectors are constant in the analyzing time window. This assumption can restrict the portion of track data where the model can be fitted such as relatively directed movement. To realize more robust estimation and deal with the temporal change of wind and heading vector, an advanced model was developed in the first part of chapter 3. The advanced model was applied to the track data of wandering albatrosses.
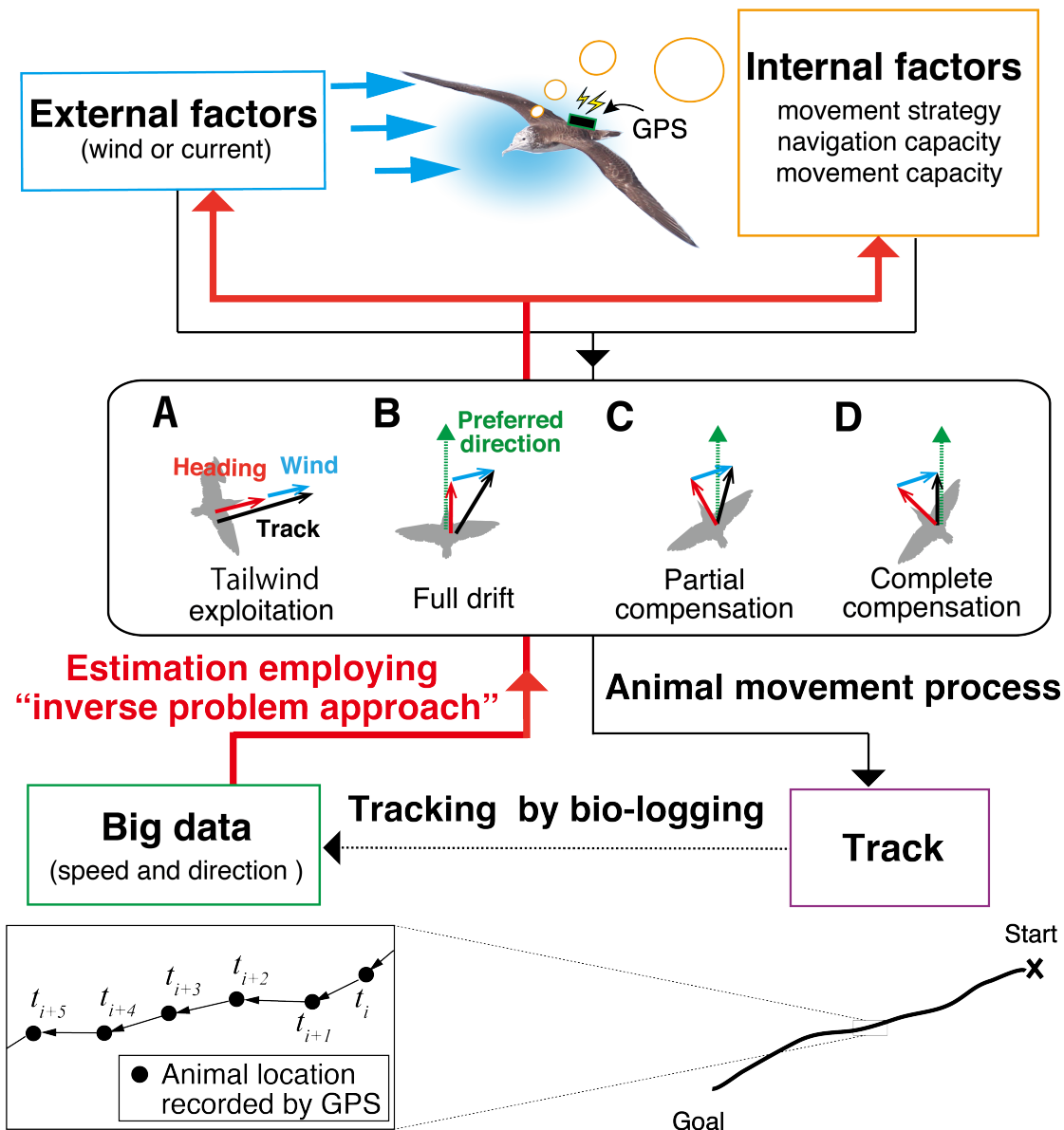
Fig. 1-1. Conceptual framework of the "inverse problem approach" with bio-logging data. The black and red arrows between boxes indicate the process by which the movement path (the line at the bottom right) of an animal is generated and how the "inverse problem approach" is applied, respectively. In general, the animal's movement is affected by both external factors (e.g., wind or currents) and internal factors (e.g., the internal state, animal navigation capacity and motion capacity). In this study, information relating to animal heading (internal factors) and ocean wind (external factors) were simultaneously estimated by analyzing time-series data recorded by bird-borne GPS loggers. (A, B, C, D) Patterns of an animal response to flow: (A) Downstream orientation. (B) Full drift. (C) Partial compensation. (D) Complete compensation. The red, blue, and black arrows from (A) to (D) indicate the heading vector, flow vector, and track vector, respectively. The green arrow indicates the preferred direction of the animal (the direction of the destination).

CHAPTER2

Seabirds' wind compensation over the sea

Introduction

In this chapter, the orientation strategy of pelagic seabirds, streaked shearwaters (*Calonectris leucomelas*: Fig. 2-1), in response to wind was investigated. Streaked shearwaters spend most of their life on/over the sea, and, in breeding season, they nest in offshore islands mainly in Japan. Streaked shearwaters breeding in Funakoshi-Ohsima Island, Iwate Prefecture, Japan was tracked using small GPS (Fig. 2-2). In breeding season, they commute between the nesting island and foraging areas of the sea to capture preys for the chicks and themselves. Sometimes, they make very long foraging trips that range to the south coast of Hokkaido (Fig. 2-2). When they return from Hokkaido to their home, they fly over the open sea approximately 300 km. As landmarks are poor over the sea, whether they can compensate wind is not obvious and important to test their navigation ability. However, the knowledge of wind compensation of birds over the sea has been very limited, although wind response of birds flying over the land (where landmarks are available) has long been studied. This is because of the technical difficulty to measure wind and heading direction of birds flying over the sea on fine-scale.

Here, a new method is proposed to estimate the heading and flow vectors to reveal animal decision-making in response to the flow, using tracking data only. For this, a model that quantitatively relates the observation data (i.e., track data) with the parameters to be estimated (i.e., heading and wind vectors) is required. Here, such a model is constructed by using a (Biased) Random Walk model, one of the basic theories for animal movement analysis that describe the direction and length of the animal track vector using probability densities. This formulation has the following three advantages: (Property 1) The model can deal with random fluctuation observed in animal movement paths (Kareiva and Shigesada 1983). (Property 2)

Variation of the probability density parameter allows the models to describe various types of movement modes, from exploratory searching to directed movement toward a particular direction or location (Codling et al. 2008). (Property 3) It is easy to fit the model to the real data and find the best-fit parameter values by formulating the maximum likelihood function and/or state-space modeling framework (Morales et al. 2004, Jonsen et al. 2013, Hooten et al. 2017). The new model is similar to previous models in respect of the above three properties, but which differs in terms of the implementation of the random walk; that is, "inversely" estimating the environmental factor (flow vector) and the internal decision making (heading vector) of animals from the "resultant" animal tracks. This method was applied to the homing tracks of streaked shearwaters and their orientation strategy over the sea was investigated.

Materials and method

The key idea of the model

First, the key point of the model, which is based on the Biased Random Walks [BRW: (Codling et al. 2010)], is explained. The BRW is a simple model for describing animal directed movement toward a particular goal direction or location. It describes the length (speed) and direction of a track vector with mutually independent probability densities and the density of the direction has a peak in the goal direction. This independency between the direction and length of the track vector assumes a symmetric distribution of the track vector along its mean. What this assumption asserts is that, when you are walking in a particular direction, there should be some degree of fluctuation in each of the steps, but the fluctuation should not be different between the left side and right side relative to the mean track direction. This assumption seems intuitively natural. However, if you are walking on moving ground, such as a glacier, your track vector (movement relative to the "earth") does not necessarily fluctuate symmetrically along its mean, but the velocity relative to the glacier should fluctuate symmetrically and thus obey the BRW. This is also the case with flying or swimming animals when an animal

is moving towards a particular destination through a moving fluid. The heading vector is distributed "symmetrically" along its mean vector (Fig. 2-3A) but the track vector should be distributed "asymmetrically" along its mean vector via the effect of the flow (Fig. 2-3B). In other words, the heading vector should obey BRW, but not the track vector. This is the key point of the method and overlooked in random walk models in movement ecology. This key point eventually enables to estimate the heading and wind vector only from track data as explained in the following sections. The model is described in the next section (The model). Then, how to apply the model to real track data (The model fitting) is described.

The model

When an animal moves while subjected to flow, its resultant track reflects the combined effects of the animal's movement relative to the fluid and drift caused by the flow. The condition is considered in which the animal's position in the x- and y-directions ($\mathbf{X}_k$) are recorded at discrete time points $k = 0,1,\ldots,N$ with the fixed time interval Δt. The animal's track vector at time point k is defined as $\mathbf{v}_{T,k} = \left(v_{T,k}, u_{T,k} \right)$, the subtraction of consecutive positions divided by the time elapsed.

$$\mathbf{v}_{T,k} \equiv \frac{\mathbf{X}_k - \mathbf{X}_{k-1}}{\Delta t} \qquad [2\text{-}1]$$

The track vector is the sum vector of the animal's heading vector at time point k, $\mathbf{v}_{H,k} = \left(u_{H,k}, v_{H,k} \right)$, and the flow vector at time point k, $\mathbf{w}_k = \left(w_{k,x}, w_{k,y} \right)$

$$\mathbf{v}_{T,k} = \mathbf{v}_{H,k} + \mathbf{w}_k \qquad [2\text{-}2]$$

The aim of the method is to estimate the mean heading vector and flow vectors from the time series of the track vector $\left\{ \mathbf{v}_{T,1}, \mathbf{v}_{T,2}, \cdots, \mathbf{v}_{T,N} \right\}$, which can be easily calculated from the tracking data. For this purpose,

$\mathbf{v}_{T,k}$ is formulated as a stochastic variable generated from a particular probability density function characterized by the heading vector and flow vector.

Followings were assumed about the heading vector and flow vector. First, heading vector $\mathbf{v}_{H,k}$ is a stochastic variable whose probability density of the length (the animal speed relative to the fluid, air-speed for flying animals, and swim-speed for swimming animals, hereafter referred to as the heading speed; $s_{H,k} = |\mathbf{v}_{H,k}|$) is not affected by that of the direction (heading; $\theta_{H,k} = \arg \mathbf{v}_{H,k}$). Second, the animal movement relative to flow is directional. In other words, the probability density of the heading has a single peak at the particular mean heading ϕ. As probability densities that satisfy these two assumptions, the Weibull distribution $f(s_{H,k}|\iota,\rho)$ is used for the heading speed,

$$f\left(s_{H,k}|\iota,\rho\right) = \rho\left\{\frac{\Gamma\left(1+1/\rho\right)}{\iota}\right\}^{\rho} s_{H,k}^{\rho-1}\exp\left[-\left\{\frac{\Gamma\left(1+1/\rho\right)s_{H,k}}{\iota}\right\}^{\rho}\right]$$

where ι is the mean heading speed, ρ is the so-called shape parameter and $\Gamma(x)$ is gamma function ; and the von-Mises distribution $g(\theta_{H,k}|\phi,\kappa)$ is used for the heading,

$$g\left(\theta_{H,k}|\phi,\kappa\right) = \frac{\exp\left\{\kappa\cos\left(\theta_{H,k}-\phi\right)\right\}}{2\pi I_0\left(\kappa\right)}$$

where ϕ is the mean heading, κ is the concentration parameter that characterizes the variance of the distribution and $I_0(\kappa)$ is the modified Bessel function of the fist kind and zero order. From these two distributions the probability density of $\mathbf{v}_{H,k} = \left(u_{H,k}, v_{H,k}\right)$, represented by $p_H\left(u_{H,k}, v_{H,k}|\iota,\rho,\phi,\kappa\right)$, can be derived.

$$p_H\left(u_{H,k}, v_{H,k}|\gamma,\rho,\phi,\kappa\right) = f\left(s_{H,k}|\gamma,\rho\right)g\left(\theta_{H,k}|\phi,\kappa\right)\left|\frac{\partial\left(s_{H,k},\theta_{H,k}\right)}{\partial\left(u_{H,k}, v_{H,k}\right)}\right|$$

where $\left|\dfrac{\partial\left(s_{H,k},\theta_{H,k}\right)}{\partial\left(u_{H,k},v_{H,k}\right)}\right|$ is the Jacobian required for the variable transformation of the probability density. Note that

it is symmetrically distributed along its mean heading vector (Fig. 2-3A). This model is the BRW which has

been widely used for modeling the "track vector" (Codling et al. 2008). However, as explained in "The key

idea of the model", it was found that the "heading vector" should obey BRW for animal movement in fluid.

The final assumption is that flow vector $\mathbf{w}_k=\left(w_{x,k},w_{y,k}\right)$ can be approximated by a spatiotemporally

constant vector $\mathbf{w}=\left(w_{x,k},w_{y,k}\right)$ during the unit of model fitting. Under the assumption of this constant flow

vector, the flow-induced drift effect usually ignored in previous models of animal movement was added.

Using the relation, $\mathbf{v}_{T,k}=\mathbf{v}_{H,k}+\mathbf{w}$ the probability density of the track vector

$p_T\left(u_{T,k},v_{T,k}\middle|\iota,\rho,\phi,\kappa,w_x,w_y\right)$ can be derived from that of the heading vector $p_H\left(u_{H,k},v_{H,k}\middle|\iota,\rho,\phi,\kappa\right)$

by transforming its variables from $\left(u_{H,k},v_{H,k}\right)$ to $\left(u_{T,k},v_{T,k}\right)$ as

$$
\begin{aligned}
&p_T\left(u_{T,k},v_{T,k}\middle|\iota,\rho,\phi,\kappa,w_x,w_y\right)\\[4pt]
&=p_H\left(u_{H,k},v_{H,k}\middle|\iota,\rho,\phi,\kappa\right)\left|\frac{\partial\left(u_{H,k},v_{H,k}\right)}{\partial\left(u_{T,k},v_{T,k}\right)}\right|\\[4pt]
&=f\left(s_{H,k}\middle|\iota,\rho\right)g\left(\theta_{H,k}\middle|\phi,\kappa\right)\left|\frac{\partial\left(s_{H,k},\theta_{H,k}\right)}{\partial\left(u_{T,k},v_{T,k}\right)}\right|\\[4pt]
&=\frac{\rho\Gamma\left(1+1/\rho\right)^{\rho}}{2\pi\iota^{\rho}I_0\left(\kappa\right)}\left\{\left(u_{T,k}-w_x\right)^2+\left(v_{T,k}-w_y\right)^2\right\}^{\frac{\rho-2}{2}}\\[4pt]
&\times\exp\left[-\left\{\frac{\Gamma\left(1+1/\rho\right)}{\iota}\sqrt{\left(u_{T,k}-w_x\right)^2+\left(v_{T,k}-w_y\right)^2}\right\}^{\rho}+\kappa\frac{\left(u_{T,k}-w_x\right)\cos\phi+\left(v_{T,k}-w_y\right)\sin\phi}{\sqrt{\left(u_{T,k}-w_x\right)^2+\left(v_{T,k}-w_y\right)^2}}\right].
\end{aligned}
$$

The equation $\left|\dfrac{\partial\left(s_{H,k},\theta_{H,k}\right)}{\partial\left(u_{H,k},v_{H,k}\right)}\right|\left|\dfrac{\partial\left(u_{H,k},v_{H,k}\right)}{\partial\left(u_{T,k},v_{T,k}\right)}\right|=\left|\dfrac{\partial\left(s_{H,k},\theta_{H,k}\right)}{\partial\left(u_{T,k},v_{T,k}\right)}\right|$ was used to transform the first line to the second line. The

equation $\left|\dfrac{\partial\left(s_{H,k},\theta_{H,k}\right)}{\partial\left(u_{T,k},v_{T,k}\right)}\right|=\dfrac{1}{\sqrt{\left(u_{T,k}-w_x\right)^2+\left(v_{T,k}-w_y\right)^2}}$ was used to convert the second line to the third line. The

$p_T\left(u_{T,k}, v_{T,k} \middle| \iota, \rho, \phi, \kappa, w_x, w_y\right)$ corresponds to $p_H\left(u_{H,k}, v_{H,k} \middle| \iota, \rho, \phi, \kappa\right)$ translated to $\mathbf{w}$ (Fig. 2-3AB). The

important prediction of the model is that the track vectors should be distributed asymmetrically along the

mean track vector (Fig. 2-3B). Note that the flexibility of Random Walk models (Property 2 mentioned in the

Introduction) enables the formulation of the animal movement in moving fluid, and the random fluctuation of

animal track described by Random Walk models (Property 1) is crucial in this model.

The model fitting

(i) Parameter estimation

When the track vector data $\left\{\mathbf{v}_{T,1}, \mathbf{v}_{T,2}, \cdots, \mathbf{v}_{T,N}\right\}$ are given, the likelihood of the model can be calculated as

follows:

$$L\left(\iota, \rho, \phi, \kappa, w_x, w_y\right) = \prod_{k=1}^{N} p_T\left(u_{T,k}, v_{T,k} \middle| \iota, \rho, \phi, \kappa, w_x, w_y\right) \qquad \text{[2-3]}$$

Using the Maximum Likelihood estimation (MLE), the parameters $\iota, \rho, \phi, \kappa, w_x$ and w_y can be

estimated (Property 3). Accordingly, the mean heading vector and flow vector can be estimated by fitting the

model to the track vector data. By conducting this estimation for the simulated movement data, the effect of a

small sample size, the fluctuation of wind, and measurement error on the accuracy of parameter estimation

was tested (MLE was conducted using "optim()" of R version 3.2.0). It was found that, in some respects, these

factors could be problematic for estimations; thus, five conditions to exclude these problems were specified

(see Supplementary Note 1 and 2 for detailed information).

Condition 1: Only one result was accepted for which the estimated probability density of the heading vector is

anisotropic and more widely distributed along the perpendicular direction relative to the axis of the mean

heading vector than along the axis of this vector (specific representation is provided in Supplementary Note 1

Eq. **S1-3**).

Condition 2: Only one result is accepted in which the angle between the mean heading and the mean track vector is less than 90 degrees.

Condition 3: Although the heading was estimated accurately, the mean heading speed widely fluctuated and deviated from the value that was obtained as an answer with only 50 data points. Accordingly, the mean heading speed l is assigned a priori. In this study, a value of 9.63 m s^{-1} (34.7 km h^{-1}) was used, which is the mean speed relative to the ground for streaked shearwaters reported in a previous work (Shiomi et al. 2012).

Condition 4: The standard deviation of the distance between the animal's true fixed position and the observed fixed position is less than 5% of the distance between successive observed fixed positions.

Condition 5: The flow fluctuation is smaller than that of the animal heading vector.

Thus, assuming condition 4 and 5 are satisfied and conducted the MLE under condition 3, fixed the mean heading speed value (l) to 9.63 m s^{-1}, and if the estimated parameters satisfied conditions 1 and 2, the goodness of model fit was checked as follows.

(ii) Goodness of fit tests

The goodness of fit of the estimated distribution of the data was verified using statistical tests. First, it was checked whether the data related to the heading and heading speed were distributed according to the estimated distributions by using a Kolmogorov-Smirnov test. Second, it was tested whether the heading and heading speed were uncorrelated by using Pearson's correlation test. If the estimated distribution passed these tests, it was accepted that the model fits the data.

Field experiment

Streaked shearwaters (*Calonectris leucomelas*) breeding at Funakoshi-Ohshima Island, Japan (Fig. 2-2) (39.240° N, 141.590° E), were tracked from August to September in 2013 and 2014, which corresponds with

the chick-rearing period. A GPS data logger was attached to each bird's back with waterproof tape (Tesa, Hamburg, Germany) and glue, (LOCTITE LBR-005, Henkel Japan, Tokyo, Japan). Two models of GPS loggers, GiPSy-2 (2013, $N = 11$ birds; 2014, $N = 14$ birds) and GiPSy-4 (2013, $N = 9$ birds; 2014, $N = 13$ birds), were used (Technosmart, Italy). GiPSy-2 was configured to record the position of the bird every minute and GiPSy-4 every 30 seconds (but resampled to 1 minute in the analysis to homogenize the sampling interval between GiPSy-2 and GiPSy-4). Recaptures of the birds at the colony to recover the loggers were began approximately 1 week after deployment. The overall mass of the logger was approximately 25 g for both models, which corresponded to less than 5% of the body mass of each bird.

Fitting the model to real track data

The foraging trips recorded by the GPS loggers were analyzed as follows. First, their homing start position was identified using a method developed in a previous study (Shiomi et al. 2012). The method defines the last phase of the track during which the distance from the colony continues to decrease as the homing phase and, in that phase, the first point where the approach speed to the colony exceeds15 km h^{-1} was defined as homing start point. Then, to eliminate the possibility that the birds used land features to navigate, only bird tracks in which the homing start position was located more than 200 km away from the colony were included for analysis. In addition, only birds that started homing further east than the longitude of the colony were analyzed. Among the recorded foraging trips, 33 trips stisfied these conditions and analyzed in the following (Fig. 2-2).

This method was applied to the homing portions of the tracks. As the animal movement pattern and flow vector are expected to change spatiotemporally, the model fitting was conducted as follows. Fifty-one minutes of position data for each bird were selected every consecutive minute in a sliding time window. Using the position data in each time window, the mean bird heading and wind (flow) vector were estimated every

consecutive minute at time point t, averaged between t-25 min to t+25 min. The bird position data were not analyzed when birds were near land, i.e., when the location of the bird at the center of the time window was closer to land than the blue dashed line, as shown in Fig. 2-2. For each time window, the track vector was derived by calculating the distance between successive GPS positions on the x- and y-axes and then dividing it by the elapsed time. As there were some missing GPS data points, the track vector was excluded from analysis when the elapsed time between points at which the GPS coordinates were fixed exceeded 1 minute. When the track vector was less than 15 km h^{-1}, the bird was assumed to be resting on the sea surface, i.e., not flying (Shiomi et al. 2012). It was ensured that the bird heading vector and wind vector were accurately estimated by fitting the model only when at least 45 over-track vector data points were contained in each window. Then, parameter estimation and goodness of fit tests for the probability density function of the bird track vector were calculated.

Comparing the wind vector estimated from bird tracks with the wind vector simulated by the atmospheric model

The validity of the model estimation was evaluated by correlating the estimated wind vectors with wind data from the Japan Meteorological Agency Mesoscale Model re-analysis datasets (at a height of 10 m above sea level), which was calculated every 3 hours. When the re-analysis data at time t was available, the mean vector of the re-analysis data was calculated and compared with the estimated wind vector at approximately time t. First, the estimated wind vectors with a time difference from t of less than 25 min were selected. The mean vector of the selected wind vector was calculated. This vector was defined as the mean estimated wind vector at time t. Next, using the wind vectors from the re-analysis data at time t, the wind vector data were selected that were within 5 km of the recorded positions of the bird from t-50 min to t+50 min except for the bird positions not contained in any time window that fit the model. The mean vector of these wind vectors was

defined as the mean re-analysis data wind vector at time *t*. The correlation between the mean estimated wind vector and the mean re-analysis data wind vector was examined using the generalized vector correlation coefficient (Crosby et al. 1993, Adams and Flora 2010) that takes into account both wind speed and direction and takes a value between 0 (no correlation) and 2 (complete correlation). The correlation of the wind speed was examined using Pearson's correlation coefficient and the correlation of the wind direction was examined using the Jammalamadaka-Sarma correlation coefficient [calculated using the package 'circular' of R (Pewsey et al. 2013)].

Testing the bird response to the wind over the sea

Using the track vector direction and the estimated bird heading direction, the degree of compensation and preferred direction were calculated by the method proposed in a previous study (Green and Alerstam 2002). First, the tracks were separated into three sections: the northern coast (NC), offshore (OS), and the western coast (WC). For each section and each track, the track vector direction and the angular difference between the track and heading vectors (α) were averaged. Then, the average track direction was linearly regressed on average α. The degree of compensation and preferred direction corresponds to the slope and intercept of the regression line (Green and Alerstam 2002). A slope of 1 signifies full drift (Fig. 1-1B), a slope of 0 means complete compensation (Fig. 1-1D), and the case 0 < slope < 1 means partial compensation (Fig. 1C).

In addition, to investigate the extent to which the preferred direction differs from that of the bird's nesting colony (i.e., the final goal), the locations with median longitude and latitude of the tracks in each section were defined as the median locations and calculated the direction of the colony from there.

Results

Model fitting to the track data

The model was applied to the homing portions of the GPS tracks of streaked shearwaters ($N = 33$; represented by the colored part in Fig. 2-2). Examples of tracks and estimated vectors are shown in Fig. 2-4ABC. Note that the asymmetry (or symmetry during light wind) of the track vector distribution predicted by the model (Fig. 2-3B) was also observed in the real data (Fig. 2-4DEF). The other three trips did not fit the model at any point and were excluded from the analysis.

Comparison between the wind vectors estimated from bird tracks and simulated by the atmospheric model

There were 32 time points at which wind vectors estimated from the bird tracks and atmospheric model matched. There was a significant correlation between the mean estimated wind vector and the mean re-analyzed data wind vector (Fig. 2-5A; generalized vector correlation coefficient =1.29 that takes a value between 0 (no

correlation) and 2 (complete correlation), $P < 0.0001$, $N = 32$). The wind speed (Fig. 2-5B; $P = 0.0019$) and direction (Fig. 2-5C; Fisher-Lee correlation coefficient 0.20, $P = 0.0013$) of the two velocities were also significantly correlated. Although the bird-based wind speed was strongly correlated with that of the re-analyzed wind data, the wind speed was 37% lower than that of the re-analyzed data (Fig. 2-5B). The difference between the bird-based wind direction and re-analyzed data was larger in light wind (Fig. 2-5D).

Wind compensation over the sea

In all three sections (NC, OS, and WC in Fig. 2-6E), the slope was significantly lower than 1 (Table 2-1, Fig. 2-6BCD), indicating that the birds were compensating for wind drift irrespective of the distance from the coastline. The degree of compensation and preferred direction differed among the sections. When birds were flying relatively near the coast (NC and WC sections in Fig. 2-6E), the slope was lower than for offshore

flight (OS section in Fig. 2-6E) and not significantly different from 0, indicating that the birds completely

compensated for wind. On the other hand, when the birds were flying over the open sea (OS section in Fig.

2-6E), the slope was significantly higher than 0, indicating that the birds partially drifted, although they still

compensated for wind to an extent (partial compensation). When the birds were flying far from the colony

(NC section in Fig. 2-6E), the direction of the colony was within 95% CI of the preferred direction. However,

when the birds flew offshore or approached the coast (OS and WC sections in Fig. 2-6E), the preferred

direction deviated from the direction of the colony in that it lay to the north of the colony (Table 2-1 and Fig.

2-6E).

Discussion

The Biased Random Walk model, the model that is commonly employed for animal directed movement,

assumed an explicitly or implicitly symmetrical distribution of the track vector along its mean vector (Codling

et al. 2008). However, the track vector should be distributed asymmetrically along its mean vector, because

flows distort the distribution. Rather, it is reasonable to assume that the heading vector is distributed

symmetrically. The wind and birds' heading vectors over the range across which the free-ranging birds moved

were obtained from GPS data only by utilizing the asymmetric distribution of the GPS track vector along its

mean vector.

Two points should be considered in relation to the method. First, the estimated wind speed was lower

than that of the reanalysis wind data. The reason for this was previously addressed (e.g., the difference in the

estimated height of ocean winds between the bird-based (less than 5 m) and satellite-based method (10 m)

(Yonehara et al. 2016)). Second, the method assumes constant heading speed (condition 3) and does not take

into account animals adjusting their heading speed in response to the wind direction and speed for

energetically optimal flight (Liechti et al. 1994, Kogure et al. 2016, Hedenström and Åkesson 2017) because

the purpose of this study is to propose a simple model and to test whether the asymmetrical distribution of the track vector contains the information of the wind and heading vectors. Although including the air speed adjustment in the model would complicate the model, it may be more realistic and valuable for future research. However, the assumption that the mean air speed of a bird is constant irrespective of wind did not affect the validity of the findings; firstly, because the estimated wind vector correlated with the reanalysis wind data sets; secondly, because the method estimated the heading direction in good precision irrespective of condition 3 as shown in the numerical simulation (see Supplementary Note 1); thirdly, because the regression method of (Green and Alerstam 2002) to estimate the preferred direction and the degree of compensation only requires the track vector direction and the heading direction that were successfully estimated (see above). Note that the airspeed was not required, which was assumed to be constant, indicating that the assumption does not affect the conclusions of shearwaters' orientation strategy.

It was showed that homing shearwaters could compensate for wind by adjusting their direction of flight such that they head into the wind depending on the degree of lateral wind. This homing behavior should be evaluated in the context of flight control and cognitive mechanism. When an animal compensates for cross winds, the animal should head in a direction away from the preferred direction. This might be easy with landmarks available; in contrast, however, it requires skillful flight-control ability when the animal is moving over the ocean surface. In particular, shearwaters and albatrosses adopt an unique flying style; dynamic soaring, i.e., the direction in which they are heading continuously changes within the scale of a few seconds (in this research, the mean values of the heading directions during a 50-min period were estimated), which makes wind compensation more demanding than that in the case of flapping birds, whose heading directions remain within a small range. Thus, the shearwaters were likely to correctly evaluate the wind conditions they experience and control their flight direction during dynamic soaring, which results in optimal navigation toward their goal.

The result also suggests the high cognitive ability of seabirds to solve an orientation task over the ocean. The possibility, known as vector orientation, could be excluded that the shearwaters continued heading in one particular direction, as turtles and the young birds of some species do (Perdeck 1958, Berthold 2001, Gaspar et al. 2006, Yoda et al. 2017). For vector orientation, only a sense of direction, i.e., the ability to detect direction using a magnetic, sun, or stellar compass, is employed. However, more complex orientation ability is required for the flow compensation the shearwaters use to return to their colony after foraging. This ability can often be termed a map sense: the ability to know where one is on the earth and the distance and direction to one's destination without any landmarks (Able 2001). As there are very few landmarks over the ocean, the finding that shearwaters compensate for the wind indicates that they possess a map sense. Their map sense over the ocean might be based on a magnetic map, olfactory map, or wave patterns (Alerstam 1976, Gagliardo et al. 2013).

The analysis also elucidated that the birds changed their orientation strategy (degree of compensation and preferred direction) during their homing. Intriguingly, the degree of compensation was higher when birds were flying over the sea near the coast (NC and WC sections) than over open sea (OS section), indicating that in the former regions they might be able to see the coast and obtain the corresponding navigational cues that were not available when flying over the open sea. In addition, the preferred direction changed with respect to the regions. The intended goal direction of birds was accurately toward the colony (final goal) at the beginning of homing flights (NC section). However, as they approached the colony (OS and WC sections), their preferred direction deviated from the colony, indicating that they tried to reach the coastline which can be used as an additional navigational cue. Thus, although birds have a map sense and can compensate for wind over the open sea, they may try to use landmarks depending on their availability.

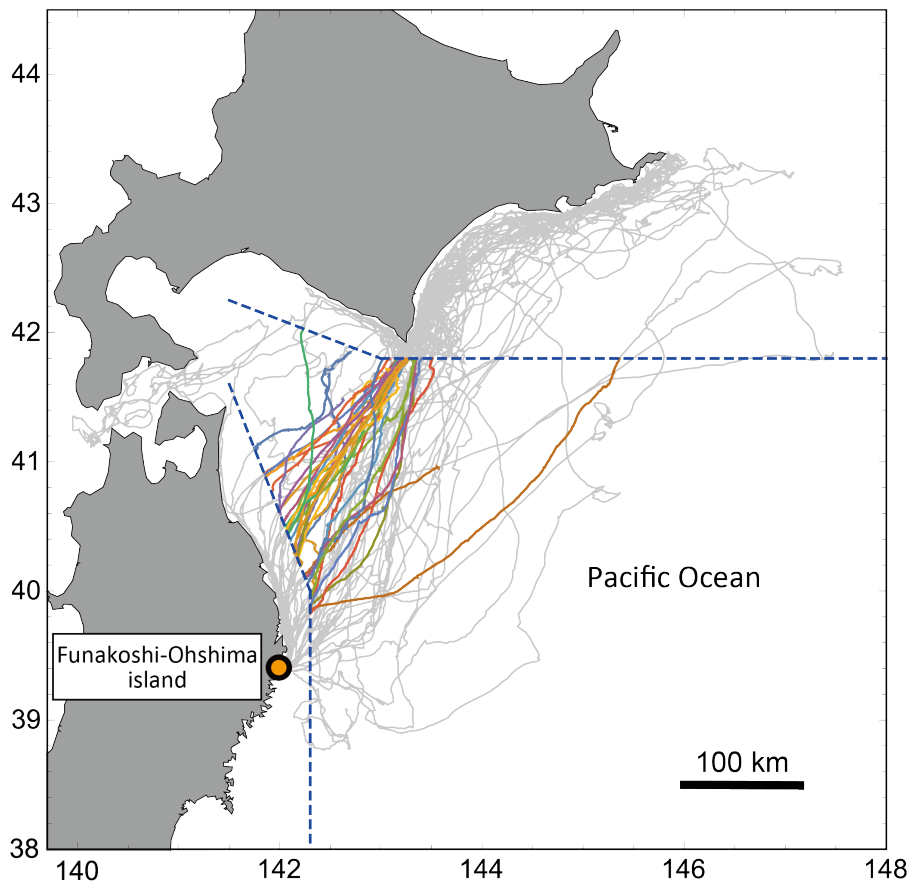**Fig. 2-1. A streaked shearwater with a data logger on its back.**

Fig. 2-2. Tracks of streaked shearwaters. Tracks of streaked shearwaters ($N = 33$). In the tracks, the parts used for analysis, i.e., those in which the bird is in the homing phase and not on land (the boundary is indicated by blue dashed lines), are indicated by colored lines. The orange dot is the nesting colony on the study site (destination).
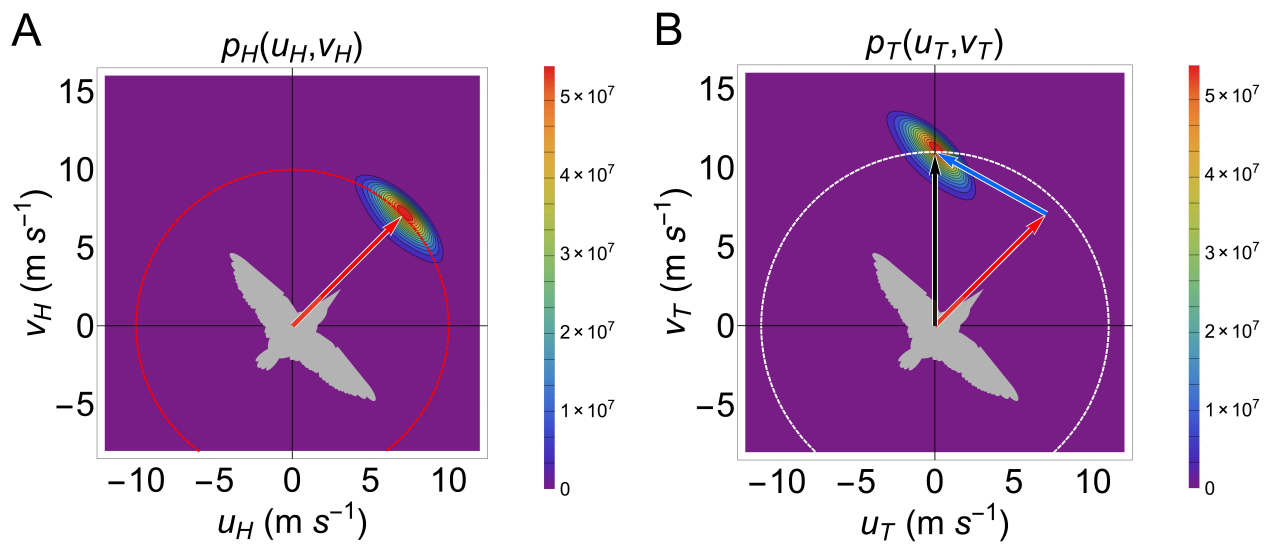
Fig. 2-3. Heading and track vector distributions of model prediction. (A) An example of probability distributions of heading vector $p_H(u_H, v_H)$, distributed symmetrically along the mean heading vector (red arrow). (B) An example of a probability distribution of a track vector $p_T(u_T, v_T)$, gained by moving $p_H(u_H, v_H)$ to the wind vector (blue arrow). It is asymmetric along the mean track vector (black arrow).
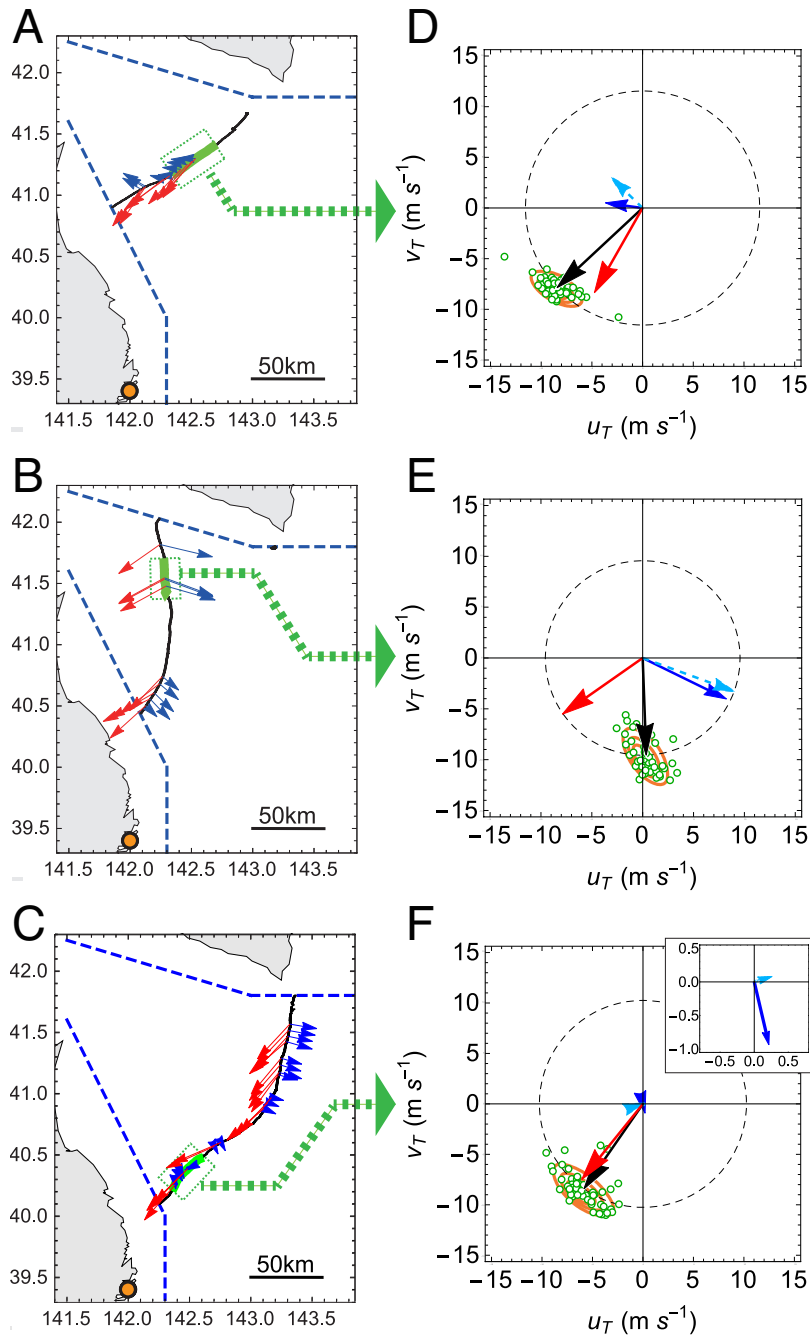
Fig. 2-4. Track vector distribution of real track. (A, B, C) The black lines, red arrows, blue arrows, and orange dots indicate the homing tracks, the estimated heading vectors, the estimated wind vectors, and the study site, respectively. (D, E, F) The track vectors calculated from the position data in the 51-min time window (the part of the track colored green in [A, B, C] is plotted [green dots]). The black, red, and blue arrows represent the mean track vector, the model-estimated mean heading vector and wind vector, respectively. The light blue dashed arrow represents the re-analysis wind data. (F) The upper right panel is a magnification of the estimated and re-analysis wind vectors in the main panel. The track vectors are distributed asymmetrically along its mean vector when a cross wind exists and almost symmetrically when the wind is weak as predicted by the model in Fig. 2-3B.

23
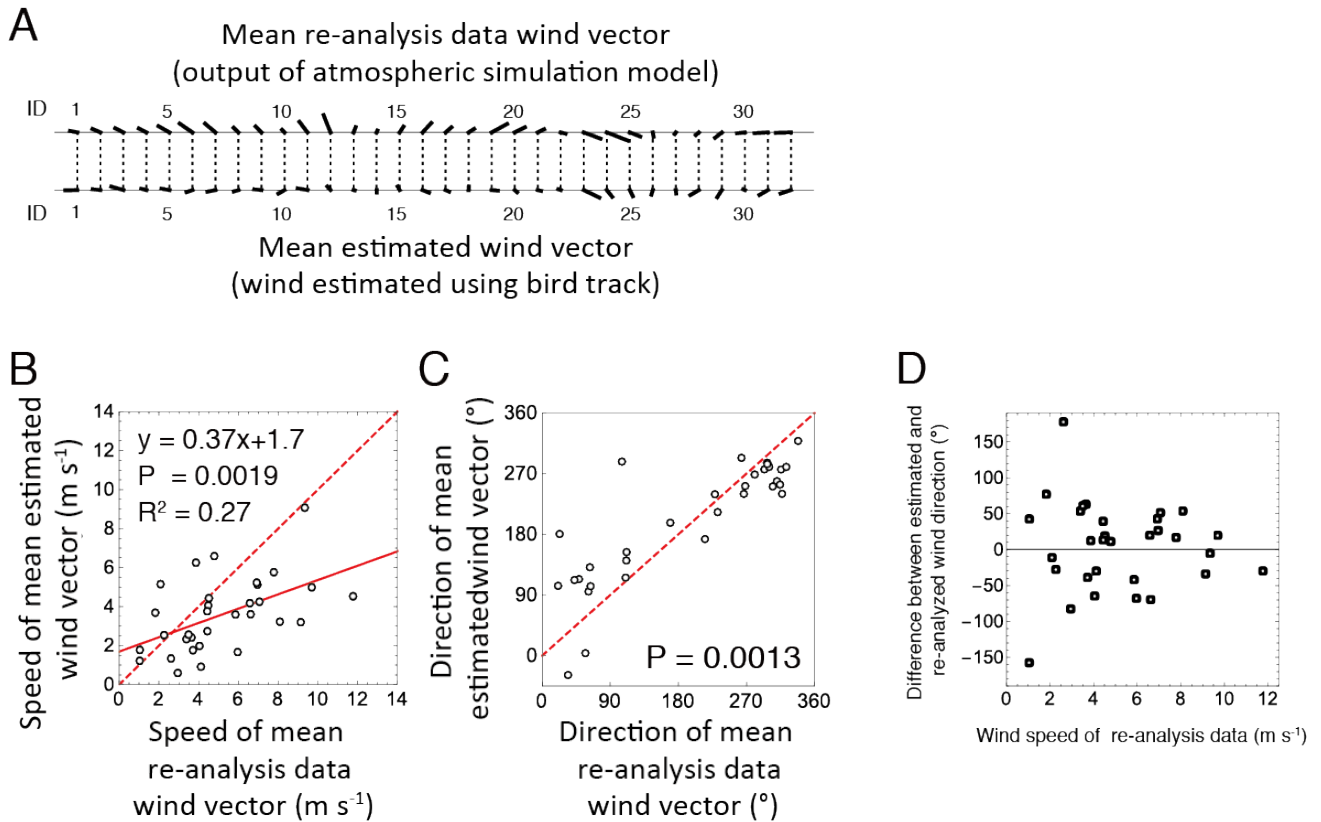
Fig. 2-5. Comparison between the wind vectors estimated by the model and by the re-analysis dataset. (A) Comparison of wind vector ($N = 32$). The first and second rows show the mean re-analysis wind vector (wind which is calculated by the atmospheric simulation model) and the mean estimated wind vector (wind which is estimated using bird tracks), respectively. The length of the line indicates the wind strength and the direction indicates the direction in which the wind blows. (B) Comparison of wind speed. The red solid line is the regression line ($y = 0.37 x + 1.7$) and the red dashed line represents $y = x$. (C) Comparison of wind direction. The red dashed line is where $y = x$. (D) Relation between wind speed and difference between estimated and re-analyzed wind direction.
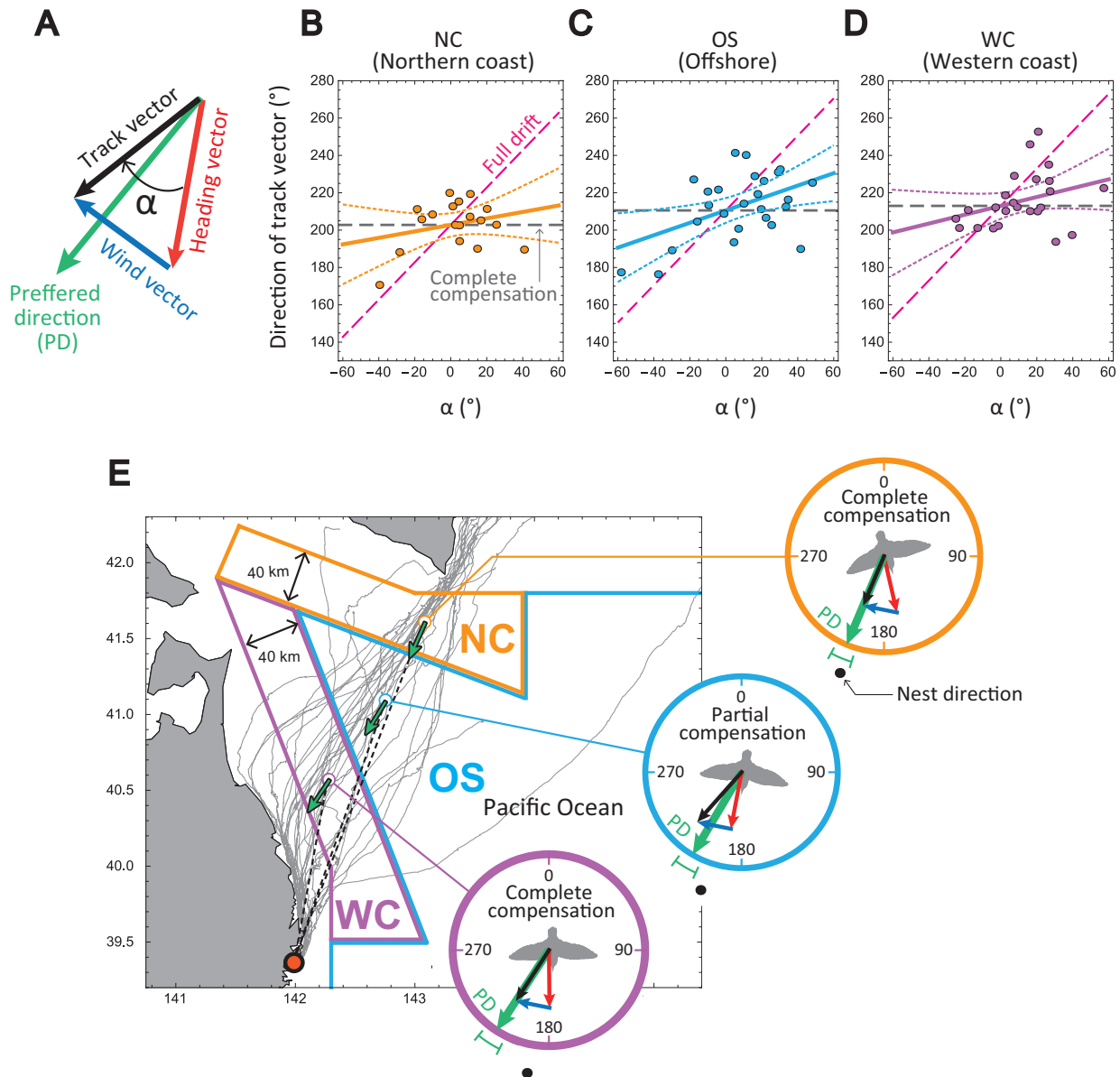
Fig. 2-6. Orientation strategies of streaked shearwaters. (A) Definition of α. (B, C, D) Mean direction of track vector plotted against α in three sections: northern coast (B), offshore (C) and western coast (D). The slope of the regression line corresponds to the degree of compensation and the intercept (the value of the track direction at $\alpha = 0$) corresponds to preferred direction. The pink dashed line (slope = 1) corresponds to birds that do not compensate (full drift) and the gray dashed line (slope = 0) indicates a bird that completely compensated for wind drift. (E) (Left side) gray lines are homing tracks and orange, light blue, and purple lines show the NC, OS, and WC sections. The orange, blue, and purple points are median locations (the location with median latitude and longitude of tracks in each sections) of the NC, OS, and WC sections. Green arrows are the preferred direction and the red point is the nesting colony (final goal). (Right side) The preferred direction (green arrows) and nest direction from the median location (black dots) in each section. The green lines are 95%CI of the preferred direction. The patterns of wind response of birds in each section are shown. The red, blue, and black arrows indicate the heading, wind, and track vector, respectively.

25

Table 2-1 Slope and intercept of the linear regression. The directions of the colony from each of the median locations (the median locations of the tracks in each of the sections. See also Fig. 6E) are also shown.

Section	N(Trip)	Slope (95% CI)	Intercept (PD) (95% CI)	Direction of the colony from the median location	R^2
Northern coast (NC)	18	0.17 (-0.15-0.50)	203° (197°-209°)	201°	0.07
Offshore (OS)	26	0.33 (0.08-0.59)	211° (204°-217°)	199°	0.23
Western coast (WC)	24	0.24 (-0.08-0.55)	213° (206°-220°)	190°	0.10

CHAPTER 3

本章の内容は学術論文として出版する計画があるため公表できない。

CHAPTER 4

本章の内容は学術論文として出版する計画があるため公表できない。

本章の内容は学術論文として出版する計画があるため公表できない。

Supplementary Notes

Supplementary Notes for Chapter 2

Supplementary Note 1: Numerical simulation test for checking the effect of realistic sample size on model fitting

Supplementary Note 2: Numerical simulation test to assess the effect of variation of flow and track location quality on model fitting

Supplementary Notes for Chapter 3

Supplementary Note 3: 公表不可

Supplementary Note 4: 公表不可

Supplementary Note 5: 公表不可

Supplementary Note 1: Numerical simulation test for checking the effect of realistic sample size on model fitting

The accuracy of parameter estimation was tested by estimating simulated movement data. Artificial track vector data, random numbers generated from the probability distribution $p_T\left(u_{T,k}, v_{T,k} \middle| \iota^*, \rho^*, \phi^*, \kappa^*, w_x^*, w_y^*\right)$ for $k=1,.., N,$ was prepared. The sample size N was set to 20, 50, or 300. $\iota^*, \rho^*, \phi^*, \kappa^*, w_x^*$ and w_y^* are parameter values used for generating artificial data. Because the accuracy of estimation is expected to depend on the shape of the probability distribution of the heading vector, a variety of heading vector distributions were simulated. The $\sigma_{H,\|}$ is defined the index to characterize the shape of heading vector probability distribution; the standard deviation of the heading vector distribution along the mean heading vector (corresponds to the standard deviation of heading speed).

$$\sigma_{H,\|} = \iota\sqrt{\Gamma\left(1+\tfrac{2}{\rho}\right)\middle/\Gamma\left(1+\tfrac{1}{\rho}\right)^2 - 1} \qquad \text{[S1-1]}$$

In addition, $\sigma_{H,\perp}$ is defined as the product of the mean heading speed (ι) and standard deviation of the heading ($\frac{1}{\sqrt{\kappa}}$; derived by approximating the von-Mises distribution as a Gaussian distribution by assuming a large value for κ), which can be regarded as the approximated standard deviation of the heading vector distribution to the perpendicular direction relative to its mean direction.

$$\sigma_{H,\perp} = \frac{\iota}{\sqrt{\kappa}} \qquad \text{[S1-2]}$$

The mean heading speed (ι^*) was set to 10 (m s^{-1}) and $\left(\sigma_{H,\|}, \sigma_{H,\perp}\right)$ to 7 combinations, which are {(1, 1), (1, 2), (2, 1), (1, 3), (3, 1)} (m s^{-1}), and the corresponding $\left(\rho^*, \kappa^*\right)$ were numerically calculated from Eq. **S1-1,2**. The probability distributions of the heading vector for each combination are shown in Fig. S1-1, which shows that these parameters characterize the variance of distribution around the mean heading vector. The mean heading and flow vector $\left(\phi^*, w_x^*, w_y^*\right)$ was set to seven combinations, as shown in Fig.

S1-2. Accordingly, 7×7=49 combinations of parameter sets were tested. Note that, for all these parameter sets, the mean track vector is the same vector whose speed is 10 m s^{-1} and direction is 0 degrees. For each parameter set, 100 data sets were generated, for each of which a maximum likelihood estimation (MLE) was conducted and the values of parameters that maximize the likelihood of the data, the so-called maximum likelihood estimates that are denoted $\iota^{(MLE)}, \rho^{(MLE)}, \phi^{(MLE)}, \kappa^{(MLE)}, w_x^{(MLE)}$, and $w_y^{(MLE)}$ were numerically computed in the following. The MLE was conducted by using the function "optim()" of R version 3.2.0. As the likelihood function may be multimodal and the estimation result may be affected by the initial values of parameters, the MLE was conducted with 12 combinations of the initial values of the parameters and selected, from the estimated parameters, the one that provides the highest likelihood as the maximum likelihood estimates. The initial value of ϕ was set from -150 degrees to 180 degrees in steps of 30 degrees. The initial value of ι was set to the mean speed relative to the ground calculated from the data. The initial value of σ was set to 15. The von-Mises distribution was fitted to the direction of artificial track vector data and used the derived concentration parameter of the fitted von-Mises distribution as the initial value of κ.

The difference between the mean heading used for generating the data and mean heading of maximum likelihood estimates, $\phi^{(MLE)} - \phi^*$, is shown in Fig. S1-3 for each combination of $\left(\sigma_{H,\parallel}, \sigma_{H,\perp}\right)$. Although the estimated mean heading was close to the true value, there were some cases in which it deviated from the true value around ± 90 or 180 degrees and the frequency of this deviation increased as the sample size decreased and the ratio $\sigma_{H,\perp}/\sigma_{H,\parallel}$ approached 1.

Two conditions were instituted to exclude cases in which the estimated headings deviated from the true values. First, only results were accepted that estimated the probability density of the heading vector to be anisotropic and were more than twice widely distributed along the perpendicular direction to the mean heading vector than along the mean heading vector (condition 1):

$$\frac{\sigma_{H,\perp}}{\sigma_{H,\parallel}} = \frac{\Gamma\left(1+\frac{1}{\rho}\right)}{\sqrt{\kappa\left\{\Gamma\left(1+\frac{2}{\rho}\right)-\Gamma\left(1+\frac{1}{\rho}\right)^2\right\}}} \geq 2 \qquad\qquad \text{[S1-3]}$$

This condition is intended to reject cases in which the heading vector distributes almost symmetrically ($\sigma_{H,\perp}/\sigma_{H,\parallel} \cong 1$) and the estimation accuracy deteriorates and also cases in which the estimated mean heading $\phi^{(MLE)}$ deviates about ±90 degrees from true value ϕ^*. This deviation means that the heading vector distribution is more widely (narrowly) distributed in the perpendicular direction than the parallel direction relative to the mean vector direction is wrongly estimated as the distribution more widely (narrowly) distributed to the parallel direction than the perpendicular direction. To exclude this miss-estimation, the direction (perpendicular or parallel) in which the heading vector distributes more widely need to be selected. As animals' heading speeds should be bounded around the particular heading speed to maintain their flight in air, the probability density of real animals' heading vector are likely to be more widely distributed in perpendicular direction than the parallel direction relative to the mean heading vector direction (which is condition 1).

Second, only results were accepted in which the angle between the mean heading and the mean track vector was less than 90 degrees (condition 2). When an estimated result does not satisfy this condition, there are two possible explanations. The first possibility is that the animal was flying against an extremely strong flow whose parallel component to the animal's heading vector was higher than the animal's heading speed, but such a situation is expected to be rare. The second, more likely, possibility is that, even though the angle between the true mean heading of the bird and the mean track vector was less than 90 degrees, the estimated heading deviated 180 degrees from the true value because of the small sample size.

Among the estimated parameter sets, results that satisfied these two conditions were selected, and the estimated mean heading and mean heading speed are shown in Fig. S1-4. If the heading vector is correctly

estimated, the flow vector is also well estimated because the flow vector is derived from subtracting the mean heading vector from the mean track vector. Although the heading is estimated accurately, the mean heading speed widely fluctuated and deviated from the value of the result. This problem is likely to stem from a small sample size and indicates that estimating the heading speed accurately with only 50 data points is difficult. Accordingly, the third condition is presented, namely that the mean heading speed ι is provided a priori (condition 3). In this study, a value of 9.63 m s^{-1} (34.7 km h^{-1}), the mean speed relative to the ground reported in previous work (Shiomi et al. 2012), was used.
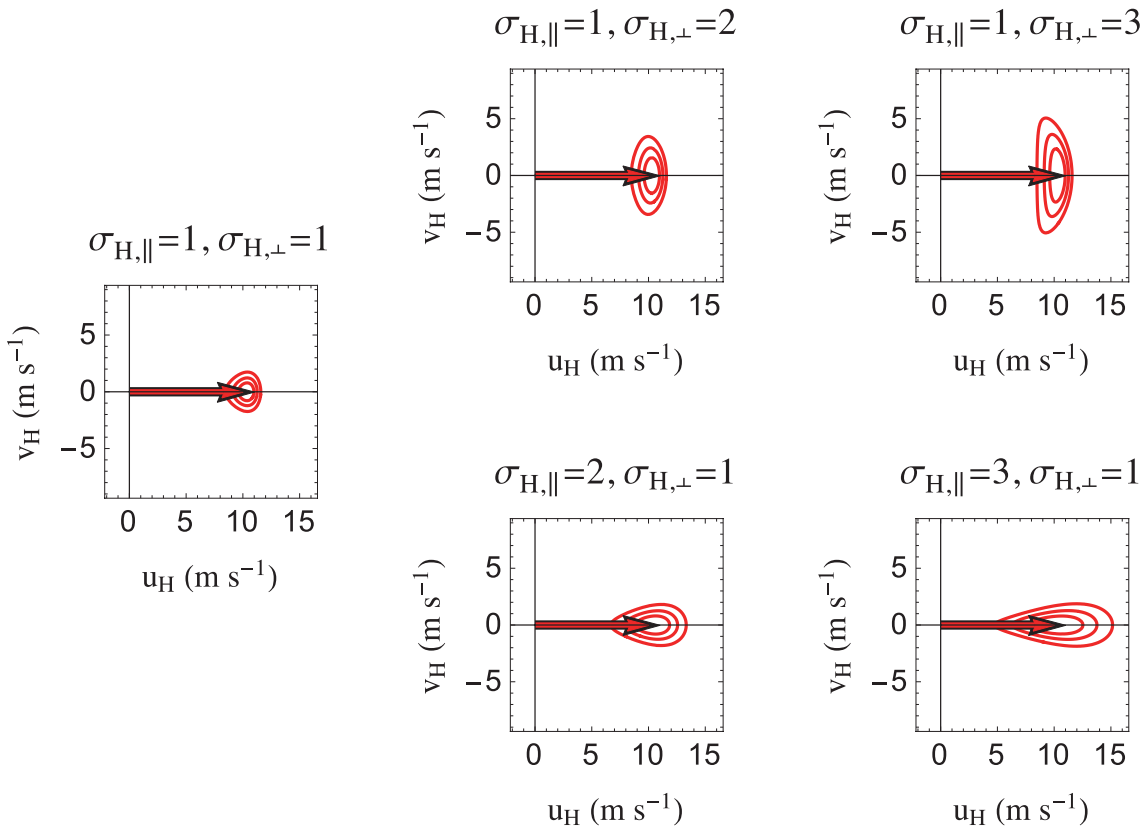
Fig. S1-1. Probability distributions of heading vector for five combinations of $\left(\sigma_{H,\parallel}, \sigma_{H,\perp}\right)$ are shown. The red circle indicates the contour lines of the distributions. The value of $\left(\sigma_{H,\parallel}, \sigma_{H,\perp}\right)$ characterizes the heading

vector fluctuation around the mean heading vector (red arrow). In this figure, the mean heading speed γ^* is set to 10 m s^{-1} and the heading ϕ^* is set to 0 as an example.
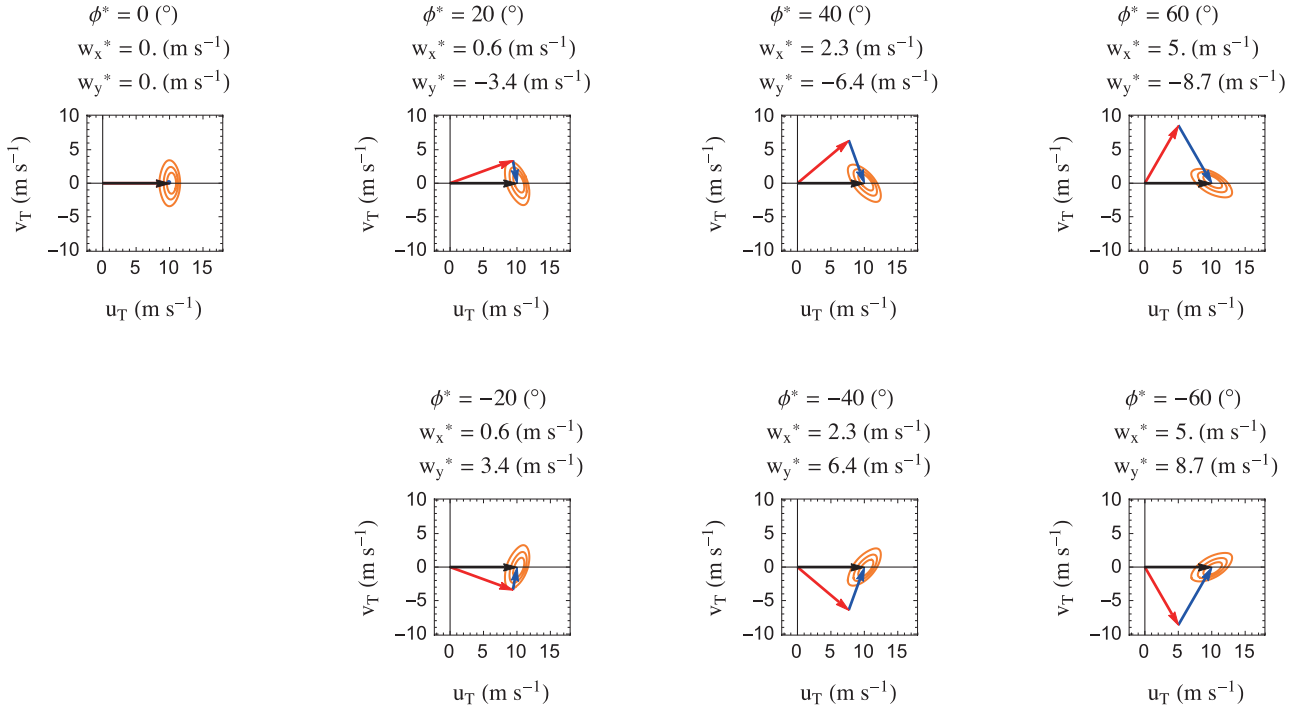
Fig. S1-2. Mean heading vector (red arrow), mean track vector (black arrow), and flow vector (blue arrow) for seven combinations of parameters $\left(\phi^*, w_x^*, w_y^*\right)$. The orange circles indicate contour lines of the examples of probability distribution of the track vector at which $\left(\sigma_{H,\parallel}, \sigma_{H,\perp}, \iota\right)$ are set to (1,2,10).
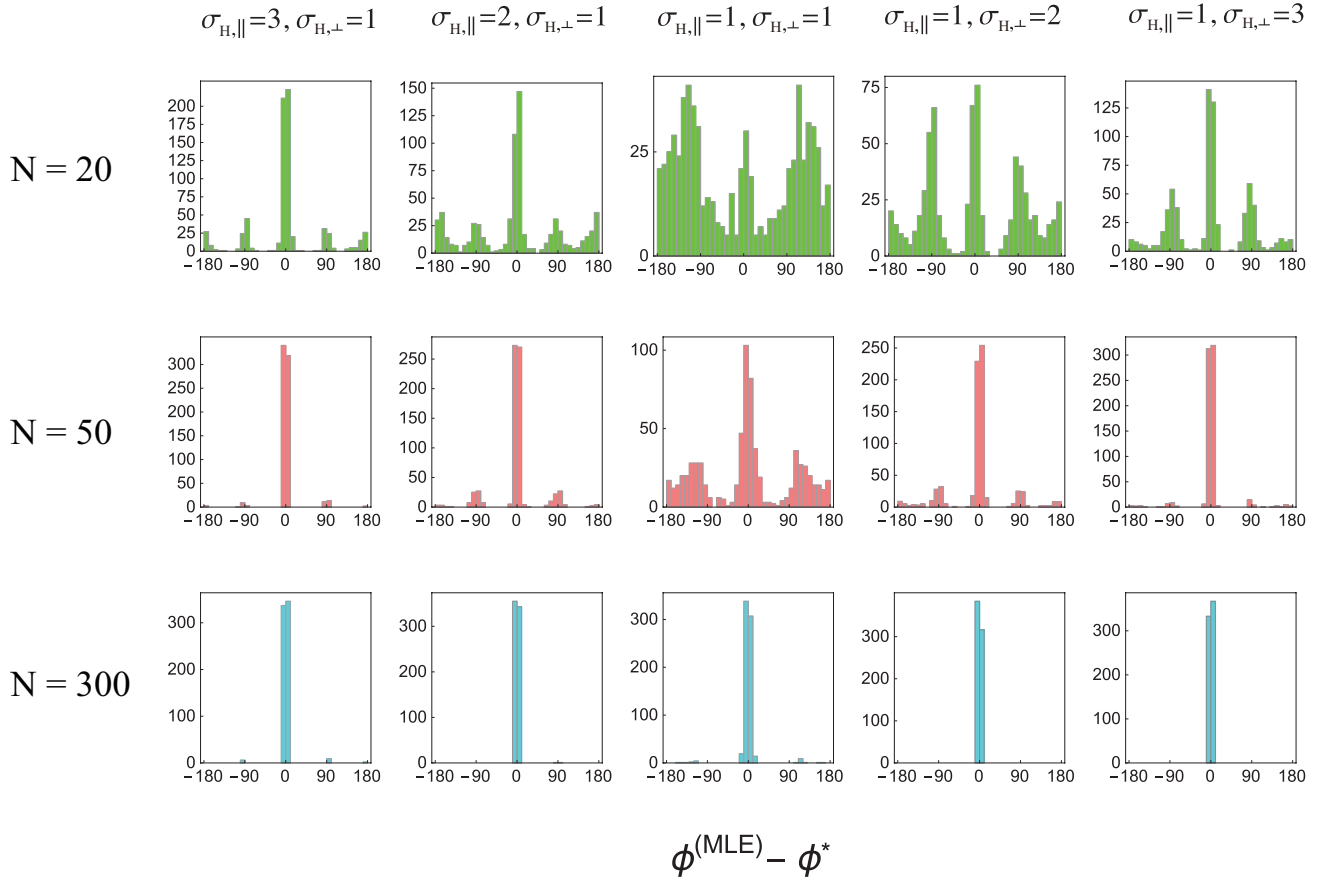
Fig. S1-3. Histogram of difference between the value of the estimated and true headings for each $\left(\sigma_{H,\|},\sigma_{H,\perp}\right)$ and sample size. The peak around zero means the heading was estimated well. There are also peaks around ± 90 and 180, which indicates the estimated heading deviated from the true value. These peaks were excluded using condition 1 and 2. As the ratio $\sigma_{H,\perp}/\sigma_{H,\|}$ deviates from 1 and as the sample size decreases, the accuracy of the estimation improves.
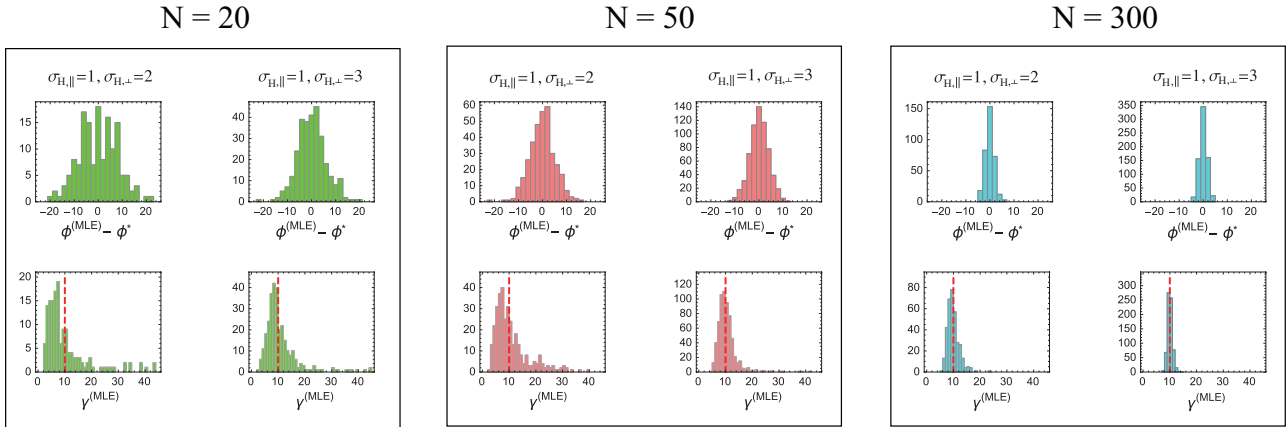
Fig. S1-4. Histograms of results that comply with conditions 1 and 2: Upper row: differences between the value of the estimated heading direction and true heading direction; Lower row: estimated mean heading speeds. Although the heading seems well estimated, the heading speeds still deviate from the true value (10 m s^{-1}; indicated by red dashed line in lower row figures). Accordingly, condition 3 was instituted.

Supplementary Note 2: Numerical simulation test to assess the effect of variation of flow and track location quality on model fitting

Although the model neglects to take into account the fluctuation of flow and the measurement error associated with fixing positions, these effects exists in real situations and affect the estimation results. The extent to which flow fluctuation and measurement error was permissible by the model was tested. Artificial track vector data that incorporated the flow fluctuation and measurement error were generated. The model was applied to these data and tested the accuracy of estimation.

The 50 points of artificial track vector data $\mathbf{v}_{T,k}$ $(k = 1,…,50)$ was generated as follows. First, heading vectors $\mathbf{v}_{H,k} = \left(u_{H,k}, v_{H,k}\right)$ $(k = 1,…,50)$ are random numbers generated from $p_H\left(u_{H,k}, v_{H,k} \middle| \iota^*, \rho^*, \phi^*, \kappa^*\right)$. Flow vectors $\mathbf{w}_k = \left(w_{x,k}, w_{y,k}\right)$ $(k = 1,…,50)$ are random numbers generated from the two-dimensional Gaussian whose mean is $\left(w_x^*, w_y^*\right)$ and the standard deviation along the mean vector direction, $\tan^{-1}\dfrac{w_y^*}{w_x^*}$, is $\sigma_{w,\|}$ and the perpendicular direction relative to mean vector is $\sigma_{w,\perp}$. Then, the observed fix at time step k, $\mathbf{X}_k^{(obs)}$, is computed, setting $X_0^{(obs)} = (0, 0)$. The measurement error is modeled by using a Gaussian distribution with standard deviation σ_{obs}.

$$X_k^{(obs)} = \left(\sum_{j=1}^{k}\left(u_{H,j} + w_{x,j}\right)\Delta t + \delta_x, \sum_{j=1}^{k}\left(v_{H,j} + w_{y,j}\right)\Delta t + \delta_y\right) \tag{S2-1}$$

$$\delta_x, \delta_y \sim N\left(0, \sigma_{obs}\right) \tag{S2-2}$$

Where Δt (sec) denotes the sampling and $N\left(a, b\right)$ denotes the Gaussian with mean a and standard deviation b. Finally, the track vector data was calculated by dividing the difference of successive fixes by elapsed time $\mathbf{v}_{T,k}^{(obs)} = \left(X_k^{(obs)} - X_{k-1}^{(obs)}\right)\Big/\Delta t$. For the mean heading vector and the mean flow vector, the seven

combinations of parameter values shown in Fig. S1-2 were used. The fluctuation of the heading vector is fixed

to $\left(\sigma_{H,\perp}, \sigma_{H,\parallel}\right)$ = (2, 0.5) (m s^{-1}). For the fluctuation of the flow vector, nine combinations of parameters are

used, $\left(\sigma_{w,\parallel}, \sigma_{w,\perp}\right)$ = {(0.25, 0.25), (0.5, 0.5), (1, 1), (0.5, 0.25), (1, 0.5), (2, 1), (0.25, 0.5), (0.5, 1), (1, 2)}

(m s^{-1}), as shown in the first column of Fig. S2-1. The observation noise is transformed as

$\sigma_{obs} = \Omega E\left(\left\|\mathbf{X}_{k+1}^{(obs)} - \mathbf{X}_{k}^{(obs)}\right\|\right)$ ($E\left(\cdots\right)$ denotes the mean value of $\cdots$. In this simulation,

$E\left(\left\|\mathbf{X}_{k+1}^{(obs)} - \mathbf{X}_{k}^{(obs)}\right\|\right) = 10\Delta t$ (m) as the mean speed relative to the ground is set to 10 m s^{-1}). Four values of

Ω as (0, 0.05, 0.1, 0.15) were tested. For example, when Ω is 0.05, the standard deviation of the distance

between the true fixed position of the animal and the observed fixed position is 5% of the distance between

successive observed fixed positions. Therefore, 7×9×4 =252 parameter sets were simulated. For each

parameter set, 50 artificial data sets were generated. The model was fitted to each data set and conducted

vector estimation following the procedure described in (i) and (ii) of the section titled "*The model fitting.*" For

each combination of flow fluctuation and the degree of observation error $\left(\sigma_{w,\perp}, \sigma_{w,\parallel}, \sigma_{obs}\right)$, seven

combinations of mean heading vector and flow vector are simulated and, accordingly, 7×50=350 trials are

conducted for each $\left(\sigma_{w,\perp}, \sigma_{w,\parallel}, \sigma_{obs}\right)$. Using the result of 350 trials, the "model fitted ratio," which is the

ratio of the trials model fitted in 350 trials, was calculated. Then, for the parameter values $\left(\sigma_{w,\perp}, \sigma_{w,\parallel}, \sigma_{obs}\right)$

whose success ratio was more than 10% of the standard deviation of the difference between the heading of

maximum likelihood estimates and the true heading ($SD\left(\phi^{(MLE)} - \phi^{*}\right)$, where SD($\cdots$) denotes the standard

deviation of $\cdots$), was calculated as the index for estimation accuracy. To calculate $SD\left(\phi^{(MLE)} - \phi^{*}\right)$ for each

$\left(\sigma_{w,\perp}, \sigma_{w,\parallel}, \sigma_{obs}\right)$, Trials were conducted for each seven combinations of the mean heading vector and flow

vector until the number of model fitted trials reached 50 and $SD\left(\phi^{(MLE)} - \phi^*\right)$ were computed using the results of 7×50 model fitted trials.

The model fitted ratio and $SD\left(\phi^{(MLE)} - \phi^*\right)$ for each $\left(\sigma_{w,\perp}, \sigma_{w,\parallel}, \sigma_{obs}\right)$ are shown in Fig. S2-1. As the observation noise increases, the model fitted ratio decreases and, if $\sigma_{obs}\Big/ E\left(\left\|\mathbf{X}_{k+1}^{(obs)} - \mathbf{X}_k^{(obs)}\right\|\right)$ exceeds 0.1, the model fitted ratio falls below 20%. Accordingly, the value of the measurement error $\sigma_{obs}\Big/ E\left(\left\|\mathbf{X}_{k+1}^{(obs)} - \mathbf{X}_k^{(obs)}\right\|\right)$ is preferred to be less than 0.05. In other words, the standard deviation of the distance between the true fixed position of the animal and its observed fixed position should be less than 5% of the distance between successive observed fixes. As the flow fluctuation increases, the model fitted ratio decreases and the $SD\left(\phi^{(MLE)} - \phi^*\right)$ increases. In particular, when the flow fluctuation is as large as the animal's heading vector, such as $\left(\sigma_{w,\parallel}, \sigma_{w,\perp}\right)$ = {(1, 1), (2, 1), (1, 2)}, the model fit was poor and estimation accuracy was low.

In conclusion, the model requires two additional conditions. The first is that the standard deviation of the distance between the true fixed position of the animal and its observed fixed position is less than 5% of the distance between successive observed fixed positions (condition 4). The second condition is that the flow fluctuation is smaller than that of the animal heading vector (condition 5).
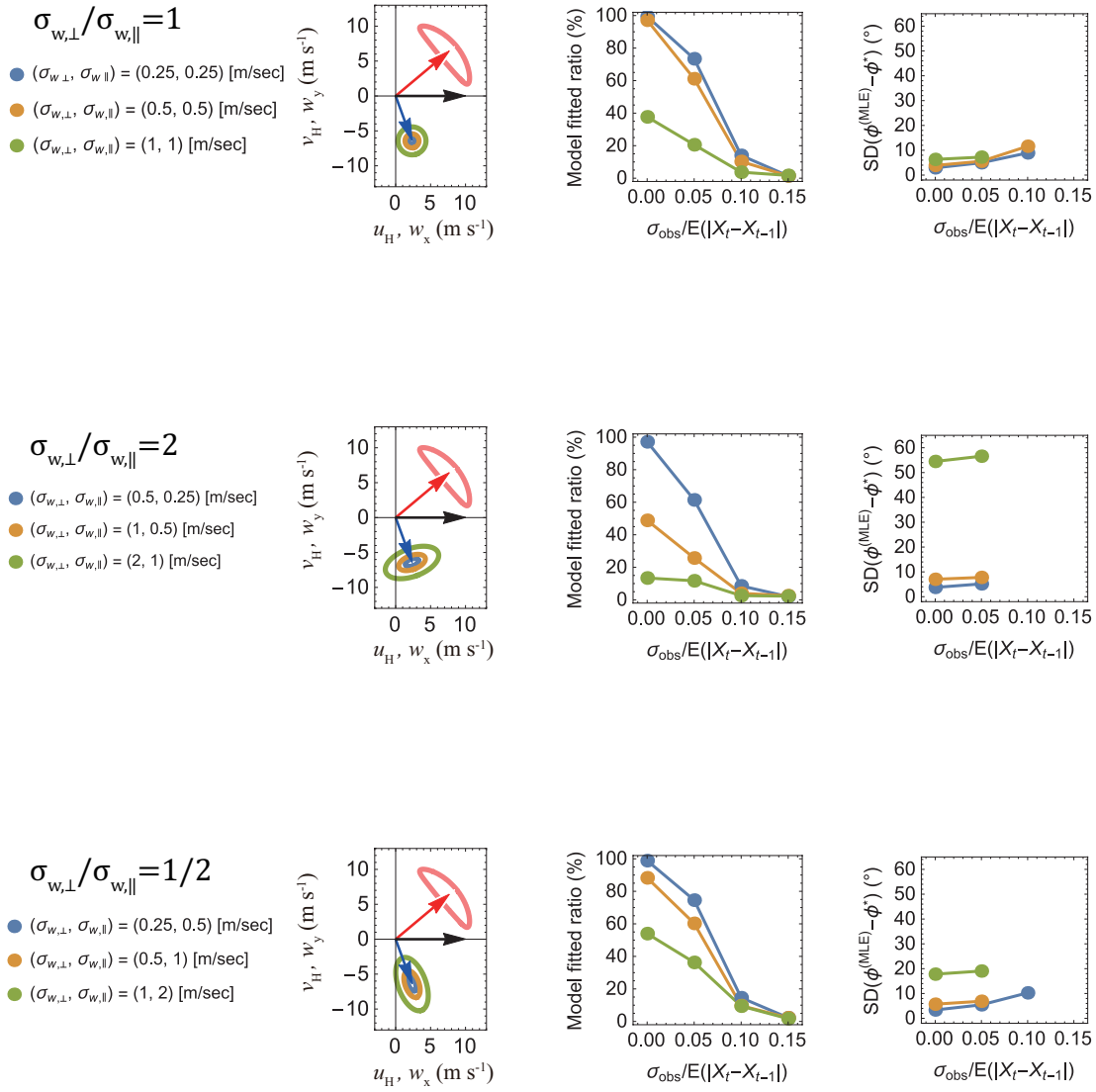
Fig. S2-1. Dependence of model fitted ratio (second column) and estimation accuracy (third column) on flow

fluctuation and location observation error. The first column shows the distribution of the heading vector and

flow vector used for simulation. The red arrow indicates the mean heading vector and the blue arrow indicates

the flow vector. The seven combinations of the mean vectors, shown in Fig. S1-2 are used for the simulation.

Supplementary Note 3: Specific representation of observation process (equation [3-8])

本章の内容は学術論文として出版する計画があるため公表できない。

Supplementary Note 4: Equation of motion for soaring birds and gliders

本章の内容は学術論文として出版する計画があるため公表できない。

Supplementary Note 5: A collocation approach

本章の内容は学術論文として出版する計画があるため公表できない。

References

Able, K. P. 2001. The concepts and terminology of bird navigation. Journal of Avian Biology 32:174–183.

Adams, J., and S. Flora. 2010. Correlating seabird movements with ocean winds: linking satellite telemetry with ocean scatterometry. Marine Biology 157:915–929.

Åkesson, S., and A. Hedenström. 2000. Wind selectivity of migratory flight departures in birds. Behavioral Ecology and Sociobiology 47:140–144.

Åkesson, S., G. Walinder, L. Karlsson, and S. Ehnbom. 2002. Nocturnal migratory flight initiation in reed warblers *Acrocephalus scirpaceus*: effect of wind on orientation and timing of migration. Journal of Avian Biology 33:349–357.

Alerstam, T. 1975. Crane *Grus grus* migration over sea and land. Ibis 117:489–495.

Alerstam, T. 1976. Do birds use waves for orientation when migrating across the sea? Nature 259:205–207.

Alerstam, T., and Å. Lindström. 1990. Optimal bird migration: the relative importance of time, energy, and safety. Pages 331–351Bird migration. Springer.

Alerstam, T., and S. Ulfstrand. 1974. A radar study of the autumn migration of Wood Pigeons *Columba palumbus* in southern Scandinavia. Ibis 116:522–542.

Alexander, R. M. 2003. Principles of animal locomotion. Princeton University Press.

Beason, R., N. Dussourd, and M. Deutschlander. 1995. Behavioural evidence for the use of magnetic material in magnetoreception by a migratory bird. Journal of Experimental Biology 198:141–146.

Benhamou, S. 2014. Of scales and stationarity in animal movements. Ecology Letters 17:261–272.

Berthold, P. 2001. Bird migration: a general survey. Oxford University Press on Demand.

Boles, L. C., and K. J. Lohmann. 2003. True navigation and magnetic maps in spiny lobsters. Nature 421:60.

Bonadonna, F., C. Bajzak, S. Benhamou, K. Igloi, P. Jouventin, H. P. Lipp, and G. Dell'Omo. 2005. Orientation in the wandering albatross: interfering with magnetic perception does not affect orientation performance. Proceedings of the Royal Society of London B: Biological Sciences 272:489–495.

Bousquet, G. D., M. S. Triantafyllou, and J.-J. E. Slotine. 2017. Optimal dynamic soaring consists of successive shallow arcs. Journal of The Royal Society Interface 14:20170496.

Butler, R. W., T. D. Williams, N. Warnock, and M. A. Bishop. 1997. Wind assistance: a requirement for migration of shorebirds? The Auk:456–466.

Chapman, J. W., R. H. G. Klaassen, V. A. Drake, S. Fossette, G. C. Hays, J. D. Metcalfe, A. M.

Reynolds, D. R. Reynolds, and T. Alerstam. 2011. Animal orientation strategies for movement in flows. Current Biology 21:R861–R870.

Chapman, J. W., C. Nilsson, K. S. Lim, J. Bäckman, D. R. Reynolds, and T. Alerstam. 2016. Adaptive strategies in nocturnally migrating insects and songbirds: contrasting responses to wind. Journal of Animal Ecology 85:115–124.

Chapman, J. W., C. Nilsson, K. S. Lim, J. Bäckman, D. R. Reynolds, T. Alerstam, and A. M. Reynolds. 2015. Detection of flow direction in high-flying insect and songbird migrants. Current Biology 25:R751–R752.

Codling, E. A., R. N. Bearon, and G. J. Thorn. 2010. Diffusion about the mean drift location in a biased random walk drift location in a biased random walk. Ecology 91:3106–3113.

Codling, E. A., M. J. Plank, and S. Benhamou. 2008. Random walk models in biology. Journal of The Royal Society Interface 5:813–834.

Crosby, D. S., L. C. Breaker, and W. H. Gemmill. 1993. A proposed definition for vector correlation in geophysics: theory and application. Journal of Atmospheric and Oceanic Technology 10:355–367.

Dänhardt, J., and Å. Lindström. 2001. Optimal departure decisions of songbirds from an experimental stopover site and the significance of weather. Animal Behaviour 62:235–243.

Dickinson, M. H., C. T. Farley, R. J. Full, M. A. R. Koehl, R. Kram, and S. Lehman. 2000. How animals move: an integrative view. Science 288:100–106.

Dodge, K. L., B. Galuardi, and M. E. Lutcavage. 2015. Orientation behaviour of leatherback sea turtles within the North Atlantic subtropical gyre. Proceedings of the Royal Society of London B: Biological Sciences 282:20143129???正しいか？.

Emlen, S. T. 1967a. Migratory orientation in the Indigo Bunting, *Passerina cyanea*. Part II: Mechanism of celestial orientation. The Auk 84:463–489.

Emlen, S. T. 1967b. Migratory orientation in the indigo bunting, *Passerina cyanea*: part i: evidence for use of celestial cues. The Auk 84:309–342.

Falkenberg, G., G. Fleissner, K. Schuchardt, M. Kuehbacher, P. Thalau, H. Mouritsen, D. Heyers, G. Wellenreuther, and G. Fleissner. 2010. Avian magnetoreception: elaborate iron mineral containing dendrites in the upper beak seem to be a common feature of birds. PLoS One 5:e9231.

Fischer, J. H., M. J. Freake, S. C. Borland, and J. B. Phillips. 2001. Evidence for the use of magnetic map information by an amphibian. Animal behaviour 62:1–10.

Fleissner, G., E. Holtkamp-Rötzler, M. Hanzlik, M. Winklhofer, G. Fleissner, N. Petersen, and W. Wiltschko. 2003. Ultrastructural analysis of a putative magnetoreceptor in the beak of homing pigeons. Journal of Comparative Neurology 458:350–360.

Fleissner, G., B. Stahl, P. Thalau, G. Falkenberg, and G. Fleissner. 2007. A novel concept of Fe-mineral-based magnetoreception: histological and physicochemical data from the upper beak of homing pigeons. Naturwissenschaften 94:631–642.

Gagliardo, A., J. Bried, P. Lambardi, P. Luschi, M. Wikelski, and F. Bonadonna. 2013. Oceanic navigation in Cory's shearwaters: evidence for a crucial role of olfactory cues for homing after displacement. Journal of Experimental Biology 216:2798–2805.

Gagliardo, A., P. Ioalè, M. Savini, and M. Wild. 2009. Navigational abilities of adult and experienced homing pigeons deprived of olfactory or trigeminally mediated magnetic information. Journal of Experimental Biology 212:3119–3124.

Gaspar, P., J.-Y. Georges, S. Fossette, A. Lenoble, S. Ferraroli, and Y. Le Maho. 2006. Marine animal behaviour: neglecting ocean currents can lead us up the wrong track. Proceedings of the Royal Society B: Biological Sciences 273:2697–702.

Goto, Y., K. Yoda, and K. Sato. 2017. Asymmetry hidden in birds' tracks reveals wind, heading, and orientation ability over the ocean. Science Advances 3:e1700097.

Green, M., and T. Alerstam. 2002. The problem of estimating wind drift in migrating birds. Journal of Theoretical Biology 218:485–496.

Groetsch, C. W. 1993. Inverse problems in the mathematical sciences. Springer.

Guisan, A., and W. Thuiller. 2005. Predicting species distribution: offering more than simple habitat models. Ecology letters 8:993–1009.

Hedenström, A., and S. Åkesson. 2017. Adaptive airspeed adjustment and compensation for wind drift in the common swift: differences between day and night. Animal Behaviour 127:117–123.

Holland, R. A., K. Thorup, A. Gagliardo, I.-A. Bisson, E. Knecht, D. Mizrahi, and M. Wikelski. 2009. Testing the role of sensory systems in the migratory heading of a songbird. Journal of Experimental Biology 212:4065–4071.

Hooten, M. B., D. S. Johnson, B. T. McClintock, and J. M. Morales. 2017. Animal Movement Statistical Models for Telemetry Data.

Ionides, E. L., C. Bretó, and A. A. King. 2006. Inference for nonlinear dynamical systems. Proceedings of the National Academy of Sciences 103:18438–18443.

Ishihara, S., and K. Sugimura. 2012. Bayesian inference of force dynamics during morphogenesis. Journal of Theoretical Biology 313:201–211.

Jonsen, I. D., M. Basson, S. Bestley, M. V Bravington, T. A. Patterson, M. W. Pedersen, R. Thomson, U. H. Thygesen, and S. J. Wotherspoon. 2013. State-space models for bio-loggers: a methodological road map. Deep Sea Research Part II: Topical Studies in Oceanography 88:34–46.

Jouventin, P., and H. Weimerskirch. 1990. Satellite tracking of wandering albatrosses. Nature

343:746.

Van Kampen, N. G. 1992. Stochastic processes in physics and chemistry. Elsevier.

Kareiva, P. M., and N. Shigesada. 1983. Analyzing insect movement as a correlated random walk. Oecologia 56:234–238.

Kogure, Y., K. Sato, Y. Watanuki, S. Wanless, and F. Daunt. 2016. European shags optimize their flight behavior according to wind conditions. Journal of Experimental Biology 219:311–318.

Kondo, Y., K. Kaneko, and S. Ishihara. 2013. Identifying dynamical systems with bifurcations from noisy partial observation. Physical Review E 87:42716.

Kramer, G. 1952. Experiments on bird orientation. Ibis 94:265–285.

Kramer, G. 1953. Wird die Sonnenhöhe bei der Heimfindeorientierung verwertet? Journal of Ornithology 94:201–219.

Lack, D. 1958. Migrational drift of birds plotted by radar. Nature 182:221–223.

Liechti, F., and B. Bruderer. 1998. The relevance of wind for optimal migration theory. Journal of Avian Biology:561–568.

Liechti, F., A. Hedenström, and T. Alerstam. 1994. Effects of sidewinds on optimal flight speed of birds. Journal of Theoretical Biology 170:219–225.

Lohmann, K. J., S. D. Cain, S. A. Dodge, and C. M. F. Lohmann. 2001. Regional magnetic fields as navigational markers for sea turtles. Science 294:364–366.

Maeda, K., K. B. Henbest, F. Cintolesi, I. Kuprov, C. T. Rodgers, P. A. Liddell, D. Gust, C. R. Timmel, and P. J. Hore. 2008. Chemical compass model of avian magnetoreception. Nature 453:387.

Maeda, K., A. J. Robinson, K. B. Henbest, H. J. Hogben, T. Biskup, M. Ahmad, E. Schleicher, S. Weber, C. R. Timmel, and P. J. Hore. 2012. Magnetically sensitive light-induced reactions in cryptochrome are consistent with its proposed role as a magnetoreceptor. Proceedings of the National Academy of Sciences 109:4774–4779.

McLaren, J. D., J. Shamoun-Baranes, and W. Bouten. 2012. Wind selectivity and partial compensation for wind drift among nocturnally migrating passerines. Behavioral Ecology 23:1089–1101.

McLaren, J. D., J. Shamoun-Baranes, A. M. Dokter, R. H. G. Klaassen, and W. Bouten. 2014. Optimal orientation in flows: providing a benchmark for animal movement strategies. Journal of The Royal Society Interface 11:20140588.

McLaren, J. D., J. Shamoun-Baranes, C. J. Camphuysen, and W. Bouten. 2016. Directed flight and optimal airspeeds: homeward-bound gulls react flexibly to wind yet fly slower than predicted. Journal of Avian Biology 46:001–015.

Miller, P. J. O., M. P. Johnson, P. L. Tyack, and E. A. Terray. 2004. Swimming gaits, passive drag

and buoyancy of diving sperm whales *Physeter macrocephalus*. Journal of Experimental Biology 207:1953–1967.

Morales, J. M., D. T. Haydon, J. Frair, K. E. Holsinger, and J. M. Fryxell. 2004. Extracting more out of relocation data: building movement models as mixtures of random walks. Ecology 85:2436–2445.

Mori, Y., and I. L. Boyd. 2004. The behavioral basis for nonlinear functional responses and optimal foraging in Antarctic fur seals. Ecology 85:398–410.

Mouritsen, H., K. P. Huyvaert, B. J. Frost, and D. J. Anderson. 2003. Waved albatrosses can navigate with strong magnets attached to their head. Journal of Experimental Biology 206:4155–4166.

Nakamura, I., Y. Goto, and K. Sato. 2015. Ocean sunfish rewarm at the surface after deep excursions to forage for siphonophores. Journal of Animal Ecology 84:590–603.

Nathan, R., W. M. Getz, E. Revilla, M. Holyoak, R. Kadmon, D. Saltz, and P. E. Smouse. 2008. A movement ecology paradigm for unifying organismal movement research. Proceedings of the National Academy of Sciences of the United States of America 105:19052–19059.

Nevitt, G. a, M. Losekoot, and H. Weimerskirch. 2008. Evidence for olfactory search in wandering albatross, *Diomedea exulans*. Proceedings of the National Academy of Sciences of the United States of America 105:4576–81.

Nießner, C., S. Denzau, J. C. Gross, L. Peichl, H.-J. Bischof, G. Fleissner, W. Wiltschko, and R. Wiltschko. 2011. Avian ultraviolet/violet cones identified as probable magnetoreceptors. PLoS One 6:e20091.

Norberg, U. M. 2012. Vertebrate flight: mechanics, physiology, morphology, ecology and evolution. Springer Science & Business Media.

Okubo, A., and S. A. Levin. 2001. Diffusion and ecological problems: modern perspectives. Springer.

Orchan, Y., O. Ovaskainen, W. Bouten, and R. Nathan. 2016. Novel insights into the map stage of true navigation in nonmigratory wild birds (Stone Curlews, *Burhinus oedicnemus*). The American Naturalist 187:E152–E165.

Patterson, T. a, L. Thomas, C. Wilcox, O. Ovaskainen, and J. Matthiopoulos. 2008. State-space models of individual animal movement. Trends in ecology & evolution 23:87–94.

Pennycuick, C. J. 2008. Modelling the flying bird. Elsevier.

Perdeck, A. C. 1958. Two types of orientation in migrating *Sturnus vulgaris* and *Fringilla coelebsas* revealed by displacement experiments. Ardea 46:1–37.

Pewsey, A., M. Neuhäuser, and G. D. Ruxton. 2013. Circular statistics in R. Oxford University Press.

Portugal, S. J., T. Y. Hubel, J. Fritz, S. Heese, D. Trobe, B. Voelkl, S. Hailes, A. M. Wilson, and J. R. Usherwood. 2014. Upwash exploitation and downwash avoidance by flap phasing in ibis formation flight. Nature 505:399.

Rayleigh, Lord. 1883. The soaring of birds. Nature 27:534–535.

Richards, P. J., A. Johnson, and A. Stanton. 2001. America's Cup downwind sails—vertical wings or horizontal parachutes? Journal of Wind Engineering and Industrial Aerodynamics 89:1565–1577.

Ritz, T., S. Adem, and K. Schulten. 2000. A model for photoreceptor-based magnetoreception in birds. Biophysical journal 78:707–718.

Sachs, G. 2004. Minimum shear wind strength required for dynamic soaring of albatrosses. Ibis 147:1–10.

Sachs, G., J. Traugott, A. P. Nesterova, and F. Bonadonna. 2013. Experimental verification of dynamic soaring in albatrosses. Journal of Experimental Biology 216:4222–4232.

Sato, K., F. Daunt, Y. Watanuki, A. Takahashi, and S. Wanless. 2008. A new method to quantify prey acquisition in diving seabirds using wing stroke frequency. Journal of Experimental Biology 211:58–65.

Sato, K., Y. Naito, A. Kato, Y. Niizuma, Y. Watanuki, J. B. Charrassin, C.-A. Bost, Y. Handrich, and Y. Le Maho. 2002. Buoyancy and maximal diving depth in penguins do they control inhaling air volume? Journal of Experimental Biology 205:1189–1197.

Sato, K., K. Q. Sakamoto, Y. Watanuki, A. Takahashi, N. Katsumata, C.-A. Bost, and H. Weimerskirch. 2009. Scaling of soaring seabirds and implications for flight abilities of giant pterosaurs. PLoS One 4:e5400.

Shaffer, S. A., H. Weimerskirch, and D. P. Costa. 2001. Functional significance of sexual dimorphism in wandering albatrosses, *Diomedea exulans*. Functional Ecology 15:203–210.

Shepard, E. L. C., R. P. Wilson, W. G. Rees, E. Grundy, S. a Lambertucci, and S. B. Vosper. 2013. Energy landscapes shape animal movement ecology. The American naturalist 182:298–312.

Shiomi, K., K. Yoda, N. Katsumata, and K. Sato. 2012. Temporal tuning of homeward flights in seabirds. Animal Behaviour 83:355–359.

Stapput, K., O. Güntürkün, K.-P. Hoffmann, R. Wiltschko, and W. Wiltschko. 2010. Magnetoreception of directional information in birds requires nondegraded vision. Current Biology 20:1259–1262.

Stelzer, R., and T. Pröll. 2008. Autonomous sailboat navigation for short course racing. Robotics and autonomous systems 56:604–614.

Stolaroff, J. K., C. Samaras, E. R. O'Neill, A. Lubers, A. S. Mitchell, and D. Ceperley. 2018. Energy use and life cycle greenhouse gas emissions of drones for commercial package delivery. Nature

communications 9:409.

Taylor, G. K., and A. L. R. Thomas. 2014. Evolutionary biomechanics: selection, phylogeny, and constraint. Oxford Series in Ecology and Evolution.

Thorup, K., T. Alerstam, M. Hake, and N. Kjellen. 2003. Bird orientation: compensation for wind drift in migrating raptors is age dependent. Proceedings of the Royal Society B: Biological Sciences 270:S8–S11.

Turchin, P. 1998. Quantitative analysis of movement : measuring and modeling population redistribution in animals and plants. Sinauer.

Videler, J. J., E. J. Stamhuis, and G. D. E. Povel. 2004. Leading-edge vortex lifts swifts. Science 306:1960–1962.

Vogel, S. 2013. Comparative biomechanics: life's physical world. Princeton University Press.

Weber, T. P., and A. Hedenström. 2000. Optimal stopover decisions under wind influence: the effects of correlated winds. Journal of Theoretical Biology 205:95–104.

Weimerskirch, H. 2007. Are seabirds foraging for unpredictable resources? Deep Sea Research Part II: Topical Studies in Oceanography 54:211–223.

Weimerskirch, H., C. Bishop, T. Jeanniard-du-Dot, A. Prudor, and G. Sachs. 2016. Frigate birds track atmospheric conditions over months-long transoceanic flights. Science 353:74–78.

Weimerskirch, H., T. Guionnet, J. Martin, S. A. Shaffer, and D. P. Costa. 2000. Fast and fuel efficient? Optimal use of wind by flying albatrosses. Proceedings of the Royal Society of London. Series B: Biological Sciences 267:1869–1874.

Weimerskirch, H., D. Pinaud, F. Pawlowski, and C.-A. Bost. 2007. Does prey capture induce area-restricted search? A fine-scale study using GPS in a marine predator, the wandering albatross. The American naturalist 170:734–43.

Wiltschko, R., I. Schiffner, and W. Wiltschko. 2009. A strong magnetic anomaly affects pigeon navigation. Journal of Experimental Biology 212:2983–2990.

Wiltschko, W., H. Höck, and F. W. Merkel. 1971. Outdoor experiments with migrating European robins in artificial magnetic fields. Ethology 29:409–415.

Wiltschko, W., U. Munro, R. C. Beason, H. Ford, and R. Wiltschko. 1994. A magnetic pulse leads to a temporary deflection in the orientation of migratory birds. Experientia 50:697–700.

Wiltschko, W., and R. Wiltschko. 1972. Magnetic compass of European robins. Science 176:62–64.

Yoda, K., T. Yamamoto, H. Suzuki, S. Matsumoto, M. Müller, and M. Yamamoto. 2017. Compass orientation drives naïve pelagic seabirds to cross mountain ranges. Current Biology 27:R1152–R1153.

Yonehara, Y., Y. Goto, K. Yoda, Y. Watanuki, L. C. Young, H. Weimerskirch, and K. Sato. 2016. Flight paths of seabirds soaring over the ocean surface enable measurement of fine-scale wind

speed and direction. Proceedings of the National Academy of Sciences of the United States of America 113:9039–9044.

Zhao, Y. J. 2004. Optimal patterns of glider dynamic soaring. Optimal control applications and methods 25:67–89.